Effect of Supernovae on the Local Interstellar Material

Priscilla Frisch and Vikram V. Dwarkadas

Abstract

A range of astronomical data indicates that ancient supernovae created the galactic environment of the Sun and sculpted the physical properties of the interstellar medium near the heliosphere. In this paper, we review the characteristics of the local interstellar medium that have been affected by supernovae. The kinematics, magnetic field, elemental abundances, and configuration of the nearest interstellar material support the view that the Sun is at the edge of the Loop I superbubble, which has merged into the low-density Local Bubble. The energy source for the higher temperature X-ray-emitting plasma pervading the Local Bubble is uncertain. Winds from massive stars and nearby supernovae, perhaps from the Sco-Cen association, may have contributed radioisotopes found in the geologic record and galactic cosmic ray population. Nested supernova shells in the Orion and Sco-Cen regions suggest spatially distinct sites of episodic star formation. The heliosphere properties vary with the pressure of the surrounding interstellar cloud. A nearby supernova would modify this pressure equilibrium and thereby severely disrupt the heliosphere as well as the local interstellar medium.

Contents

P. Frisch (✉) • V.V. Dwarkadas
Department of Astronomy and Astrophysics, University of Chicago, Chicago, IL, USA
e-mail: frisch@oddjob.uchicago.edu; vikram@oddjob.uchicago.edu

1   Introduction

Nearly a century ago, Harlow Shapley (1921) noticed that the Sun is traveling away from Orion and speculated that variations in the brightness of Orion stars could result from encounters between the stars and nebulosity that would "gravely affect the atmosphere surrounding any attendant planet." By analogy, he suggested that were the Sun to encounter diffuse nebulosity, it could induce severe changes in the terrestrial climate. Such an idea is not farfetched. Supernovae and winds from massive stars inject large amounts of energy into the interstellar medium and reshape and remix interstellar material with shock waves and expanding bubbles. Nearby supernovae occur at rates that are larger than the galactic average due to the solar location inside of Gould's Belt. The flux of galactic cosmic rays into the terrestrial atmosphere depends on the response of the heliosphere to the ambient interstellar medium (Florinski and Zank 2006; Müller et al. 2006). Geologic records indicate that cosmic rays from supernova have penetrated to the surface of the Earth (Brakenridge 1981). The Sun is traveling toward the constellation of Hercules at a velocity of ~ 18 pc per Myr through the local standard of rest (LSR) (Frisch et al. 2015). Without question the supernovae that generated the Loop I superbubble (Berkhuijsen et al. 1971) affected the ambient interstellar medium and possibly the interplanetary environment of the Earth. Locations of many supernovae within 400 pc and over the past ~ 2 Myr have been identified.

The Sun is immersed in a small, <15 pc, cluster of low density partially ionized interstellar cloudlets of the type that were once identified as the "intercloud medium" because of the low extinctions, $E(B - V) < 0.001$ mag. Most local gas is warm, $T = 5000 - 12{,}500$ K, low density partially ionized gas with log $N(HI) < 18.7$ cm^{-2}, $<n_{HI}> = 0.01 - 0.10$ cm^{-3}, and $n_p \sim 0.1$ cm^{-3} (e.g., Frisch et al. 2011; Redfield and Linsky 2004; Rogerson et al. 1973). A magnetic field with strength $\sim 3\,\mu$G shapes the heliosphere (Schwadron et al. 2011; Slavin and Frisch 2008). The only known local cloudlet that is cold and neutral is the filamentary Local Leo Cold Cloud (LLCC) dust cloud at distance ~ 18 pc (Meyer et al. 2012; Peek et al. 2011).
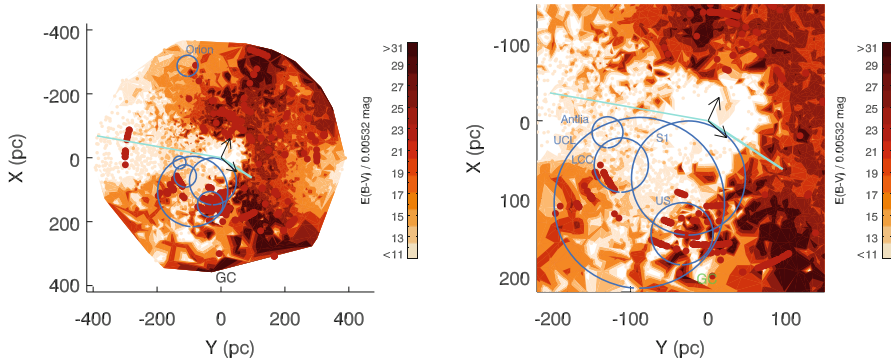
Fig. 1 The Local Bubble: The cumulative extinction of interstellar dust is shown over spatial scales of ∼300 pc (*right*) and ∼800 pc (*left*) projected onto the galactic plane (from Frisch et al. 2016). The galactic center is at large positive values of X, and the galaxy rotates toward positive Y values. The cumulative extinction is determined from the color excess E(B − V) measured for each star where the astrometric distances are required to agree with distances obtained from E(B − V) and the spectral type of the star (See Frisch et al. 2015 for more information). The *color bar* shows color excess E(B − V) in units of 0.00532 mag. *Round dark maroon circles* show the locations of nearby molecular CO clouds. The two *black arrows* show the LSR velocities of the CLIC (perpendicular to the S1 shell) and the Sun (roughly tangential to the S1 shell). The long and short *cyan-colored lines* show the directions of the interarm magnetic field and IBEX Ribbon magnetic field directions, respectively (Frisch et al. 2015; Funsten et al. 2013). The *circles* show the three superbubble shells in Sco OB2, the Antlia SN remnant, and the Ori-Eri superbubble (*left figure* only), and the S1 shell (See text for details)

This review discusses the configuration of massive stars, Gould's Belt, that spawns nearby supernovae (Sect. 2), bubble formation (Sect. 3.1), the location of the Sun inside a superbubble rim (Sect. 3.4) that merges into the low density Local Bubble cavity (Sect. 3.3), the Orion superbubble (Sect. 3.5), short-lived radioisotope clocks of recent nearby supernova found in geological and astrophysical data (Sect. 4), and the impact of supernovae on the heliosphere (Sect. 5).

The Local Bubble is characterized by a cavity in the interstellar medium (ISM). Figure 1 shows the distribution of interstellar material within ∼400 pc according to the cumulative reddening of starlight as measured by the color excess E(B − V) (Frisch et al. 2016). Superimposed on the reddening maps are nearby superbubble shells, the interarm interstellar magnetic field (ISMF) indicated by pulsar data (Salvati 2010), and the local ISMF direction diagnosed by the Ribbon of energetic neutral atoms (ENAs) discovered by the Interstellar Boundary Explorer (IBEX) spacecraft (Funsten et al. 2013; Heerikhuisen et al. 2010; McComas et al. 2009; Schwadron et al. 2009; Zirnstein et al. 2016). The extinction void around the Sun, denoted the Local Bubble, occurs where the interior of Gould's Belt blends into the interarm regions of the third galactic quadrant.

2   Gould's Belt and Massive Stars

Nearby clusters of O–B2.5 massive stars that are progenitors of core-collapse Type II and Type Ib/c supernovae form a thin planar ring-like structure around the Sun known as "Gould's Belt" (Bobylev 2014; Grenier 2004; Perrot and Grenier 2003). Gould's Belt is part of a large-scale warp in the distribution of young stars in the galactic plane (Alfaro et al. 1991). The traditional configuration of Gould's Belt as an inclined plane defined partly by the Sco OB2 and Orion OB1 associations is shown in Fig. 2 (from Grenier 2004). Gould's belt is tilted by an angle of $\sim$17.2° with respect to the galactic plane, with the ascending node toward $\sim$296° and centered $\sim$104 pc away toward $\ell \sim 184°$, where the uncertainties arise from the different selection criteria for testing the Gould's Belt configuration (Bobylev and Bajkova 2014; Grenier 2004; Perrot and Grenier 2003; Stothers and Frogel 1974). An alternate perspective compares the distribution and kinematics of open clusters in the Orion OB1 association with those of Sco OB2 to characterize Orion OB1 as belonging to the Local Arm where high densities of open clusters and ongoing star formation appear, in contrast to the Sco OB2 stars that are located on the outskirts of the Local Arm with lower densities of active star-forming regions (Alfaro et al. 2009; Elias et al. 2009). Elias et al. (2009) establish that the Local Bubble region around the Sun is devoid of open clusters in comparison to the Orion region. Bobylev and Bajkova (2014) used astrometric data to define the Orion arm as a narrow ellipsoid directed toward $\ell = 77.1° \pm 2.9°$ with a symmetry plane inclined to the galactic plane by $5.6° \pm 0.2°$ and with a longitude of the ascending node of the
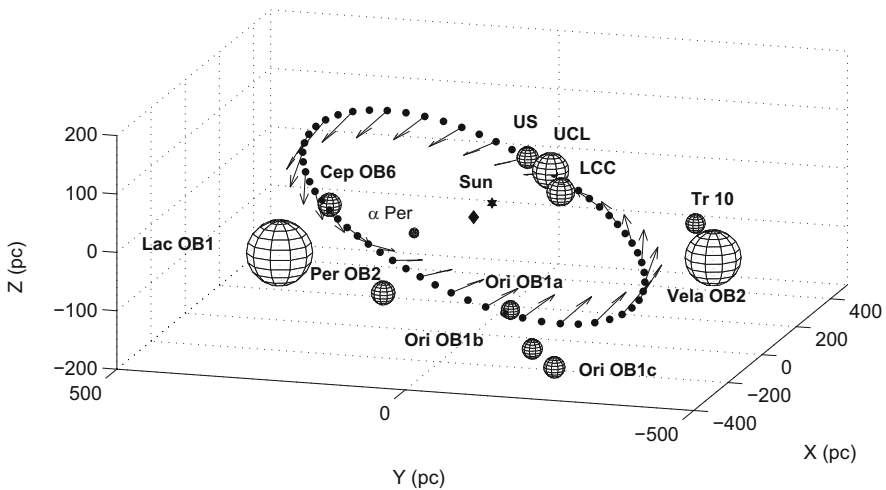

Fig. 2 Gould's Belt: Stellar associations of Gould's Belt and the velocity field of *the stars* with respect to the LSR are shown in 3D. The *diamond* shows the center of Gould's Belt, and *the star* shows the location of the Sun. The galactic center is directed toward large positive values for the x-coordinate (Figure from Grenier 2004)

plane toward $70° \pm 3°$. Regardless of the detailed description of Gould's Belt versus the Local Arm, most of the early-type O–B2.5 massive stars in the solar vicinity coincide with the traditional configuration of Gould's Belt.

About 17–20 supernovae per million years formed in the entire Gould's Belt during the past several million years, which is a rate 3–4 times that of the local galactic average (Grenier 2004). Since 80% of galactic supernova are from the core collapse of massive stars, the SNe in Gould's Belt will account for the most likely supernovae to have shaped the physical properties of the local interstellar medium. Over tens of millions of years, these supernovae have rearranged the interstellar material near the Sun into the networks of filaments, arcs, shells, and superbubbles that are observed (Cox 2005; Heiles 1979, 1984).

3   Supernova Remix of the Interstellar Medium

Superbubble shells, either complete or incomplete "worm" or filamentary structures, are common in the ISM and are nearly all explained by energy injection from stellar winds and supernovae (Heiles 1984). Measurements of the Zeeman splitting of the HI 21-cm line show that morphologically distinct filaments generally consist of warm neutral or partially ionized gas where magnetic pressure dominates thermal pressures by a factor of $\sim$67 and turbulent pressure by a factor of $\sim$10 (Heiles 1989). The rapid evolution of massive stars in Gould's Belt has frequently altered the ISM in the solar neighborhood.

3.1   Bubbles and Superbubbles

Supersonic winds from massive stars can evacuate large regions of space around the star, with radii of several parsecs. The detailed structure of these "wind-blown bubbles" was first elucidated by Castor et al. (1975) and Weaver et al. (1977) and has been subsequently refined and discussed by many authors (Koo and McKee 1992a,b; McKee et al. 1984). In general, the bubbles consist of a very low density ($<$0.01 particles cm^{-3} on average) interior surrounded by a dense shell of material, bounded by a radiative shock that serves as the boundary of the bubble. The bubbles can be either density or ionization bounded – if the shell is dense enough, an ionization front will be trapped in the dense shell, beyond which neutral material can be found. The ISM magnetic field can also affect the size, shape, and evolution of circumstellar bubbles (van Marle et al. 2015). Weaver et al. (1977) showed that the radius of the bubbles primarily grows with time as $R_b \propto \left[\frac{L}{\rho}\right]^{1/5} t^{3/5}$ where $L = 0.5\dot{M}v_w^2$ is the mechanical luminosity of the wind with mass-loss rate $\dot{M}$ and wind velocity v_w, and ρ is the density of the ambient medium.

Numerical simulations have been successful in confirming the analytical predictions and reproducing the general structure, formation, and morphology of

massive star bubbles (Dwarkadas 2007; Freyer et al. 2003, 2006; Garcia-Segura et al. 1996a,b). Other simulations have explored the evolution of the subsequent supernova shock waves within the bubbles (Dwarkadas 2005, 2007; Rozyczka et al. 1993; Tenorio-Tagle et al. 1991, 1990; van Marle et al. 2010). Although the highly supersonic winds around massive stars (wind velocity on order 1000–2000 km s^{-1}) and the low density and high pressure pervading the bubble would point to an extremely high temperature within the bulk of the bubble (of order 10^7 to 10^8 K), X-ray observations have shown that if hot gas is detected at all, its temperature and emission measure are both low, on the order of a few times 10^6 K (Chu et al. 2003a,b; Toalá et al. 2015, 2016). Many authors have tried to simulate these observations to understand the origin of the low temperatures, with some degree of success in matching the bubble temperatures and their X-ray spectra (Dwarkadas and Rosenberg 2013, 2015; Toalá and Arthur 2011).

Clusters of massive stars group together to form an association. The correlated supernovae resulting from the explosion of these stars can form even larger bubbles due to the combined effects of the winds and supernova explosions. The aptly named superbubbles (Mac Low and McCray 1988; Mac Low et al. 1989; Yadav et al. 2016) rearrange the morphology and physical characteristics of the surrounding ISM. Heiles (1979) defines bubbles with injected energies greater than 3×10^{52} ergs as supershells or superbubbles. The structure of these superbubbles is similar to their smaller brethren and can be approximated from the bubble theory allowing for continuous energy input from an association of stars and their resulting SNe. Mac Low and McCray (1988) have shown that the bubble approximation is valid even for superbubbles and show that the superbubble radius can be written as $R_{sb} \sim 267 \left[\frac{L_{38} t_7^3}{n_0} \right]^{1/5}$ pc, where L_{38} is the mechanical luminosity in terms of 10^{38} ergs s^{-1}, t_7 is the time in units of 10^7 years, and n_0 is the atomic number density. Due to their extremely large size, it is clear that these bubbles are not expanding in a homogeneous interstellar medium but in a medium whose structure is constantly being stirred due to heating by supernova explosions (Korpi et al. 1999).

The expanding flow sweeps up interstellar material and magnetic fields into a postshock shell. The mass within the bubble interior is likely regulated by evaporation from the cool bubble walls, by entrainment and ablation from denser clouds remaining within the bubble, and by the penetration of ambient interstellar clouds that are not destroyed by the photoevaporative effect of the massive star (Oey and García-Segura 2004; Shull 1993). A superbubble shell thickens as it sweeps up magnetic field lines during the pressure-driven snowplow stage, producing regions in the evolved shell where the ISMF is perpendicular to the gas velocity (Ferriere et al. 1991; Hanayama and Tomisaka 2006; Mac Low 1999), such as is found for the immediate solar environment (Sect. 3.4). For a cylindrical model with the ISMF parallel to the axis of the cylinder, superbubble expansion parallel to the radial direction produces a configuration where gas velocities are perpendicular to the ISMF direction (Hanayama and Tomisaka 2006).

It is in the context of these known bubbles that superbubbles in our vicinity, and the detection of a low-density, high-temperature region around our solar system, the Local Bubble, need to be evaluated.

3.2   Radio Superbubbles and Magnetic Loops

The closest superbubbles that have influenced the local ISM occurred in the Sco-Cen association and were first revealed through observations of the intense radio continuum source known as the North Polar Spur (NPS), a radio emission source extending north from longitude $\ell \sim 30°$. The NPS was part of a loop-like structure with a nonthermal continuum that was modeled as a supernova remnant with a 3% probability of being closer than 100 pc (Davies 1964; Hanbury Brown et al. 1960). Berkhuijsen (1971), and Berkhuijsen et al. (1971) identified four nonthermal radio loops at 830 MHz, Loops I–IV, with the NPS the brightest part of Loop I (see early review by Salter 1983). The strongly polarized radio Loop I (64% to 72% polarization) indicates a magnetic field that is uniform in direction (Heiles et al. 1980). Loops II and III are radio continuum features (Berkhuijsen 1971; Kun 2007), while Loop IV is centered on the nearby B1V star Spica (81 pc) and coincides with an Hα emission feature and hole in the HI gas that indicate Loop IV does not have a supernova origin (Reynolds 1984). Using sky maps from the Wilkinson Microwave Anisotropy Probe (WMAP) at 23, 33, and 41 GHz, Vidal et al. (2015) identified the original four loops and eleven new nonthermal loop structures, some prominent only through polarization. The mean spectral index for the brightness temperature of the polarized emissions is -3.06 ± 0.02, verifying the synchrotron nature of the emission from these radio loops.

Filling in the picture of the influence of supernova on the local ISM requires data on the neutral ISM. Heiles (1979) identified sixteen stationary HI shells within 500 pc that have diameters $\leq 36°$. Eleven large interstellar shells beyond 500 pc were termed "supershells." Radio recombination lines showed that warm, 7000 K, partially ionized filamentary structures are common through the ISM (Heiles et al. 1996).

The largest diameter radio bubble in the sky is Loop I. Successive epochs of star formation in the parent molecular cloud of Sco OB2 created large-scale nested interstellar HI shells that have provided the basis for linking nearby bubble-like structures, such as Loop I, with the parent clusters of stars (Crawford 1991; de Geus 1991). Polarization data suggest these nested shells are closer to the Sun, (at a distance ∼100 pc), in the region $20° < \ell < 40°$ than in the region $290° < \ell < 310°$ where distances are >200 pc (Santos et al. 2011). The three subgroups of the Scorpius-Centaurus association (Blaauw 1964) are the Upper Centaurus-Lupus (UCL) with a nuclear age of 14–15 Myr, Lower Centaurus Crux (LCC) with a nuclear age of 11–12 Myr, and Upper Scorpius (US) with a nuclear age of 4–5 Myr (de Geus 1992, see Fig. 1). When stellar proper motions are included, it is seen that the shell-forming events did not occur at the present locations of the stellar subgroups, and the LCC is the most likely source of the large-scale Loop I feature (Maíz-Apellániz 2001). Frisch (1981) pointed out that the low-density interarm-type material near the Sun would have led to asymmetric expansion of Loop I. The X-ray remnant toward the NPS would have resulted from star formation triggered by the impact of a shock wave on the Aquila Rift dark cloud (Crawford 1991; de Geus 1991, 1992). Iwan (1980) found that a reheated supernova remnant was required to simultaneously explain the Loop I HI radio shell and the ridge of X-ray plasma,
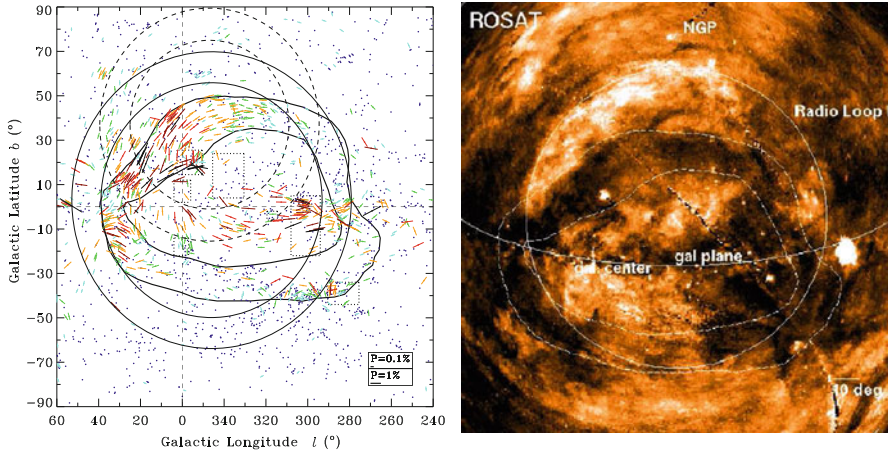
Fig. 3 *Left*: Polarized starlight toward Loop I: The optical polarizations that trace the ISMF in the neutral gas that shadows the soft X-ray background (*right*) are shown together with the S1/S2 superbubble shells (*solid/dashed circles*, respectively) from Wolleben (2007). The irregular lines reproduce the boundaries of the "interaction ring" shown at right. Figure from Santos et al. (2011). *Right*: Egger interaction ring – soft X-ray shadow appearing in ROSAT data in the energy range 0.1–2.0 keV. The X-ray shadow is caused by neutral gas with a density of $\sim 15\,\mathrm{cm^{-3}}$ that is accompanied by aligned dust grains that polarized background starlight between two interstellar bubbles with a density of $\sim 15\,\mathrm{cm^{-3}}$ that is accompanied by aligned dust grains that polarize background starlight between two interstellar bubbles. Also identified are the location of Loop I (*solid white line*), the interaction ring between the Local Bubble plasma and the Loop I bubble (outlined by *dashed lines*), and the galactic landmarks. The X-ray shadow corresponds to column densities that jump from $N(H) \sim 10^{20}$ to $7 \times 10^{20}\,\mathrm{cm^{-2}}$. Optical and UV data indicate a neutral wall with $N(H) \sim 10^{20}\,\mathrm{cm^{-2}}$ at a distance of 40 ± 25 pc (Figure from Egger and Aschenbach 1995 and courtesy of the Max-Planck-Institut fur extraterrestrische Physik (http://www.mpe.mpg.de))

although she could not incorporate the then unknown foreground contamination of the X-ray background by solar wind charge-exchange with interstellar neutrals (Koutroumpa et al. 2009).

Several recent studies (Lallement et al. 2016; Sofue 2015) attribute features generally associated with Loop I to the gamma-ray bubbles around the galactic center discovered by Fermi-Lat (Su et al. 2010), which is a viable hypothesis only because the Fermi bubbles extend $\pm 50°$ north/south of the galactic center (Su et al. 2010). These arguments rely partly on the latitude dependence of the X-ray emission compared to that of dust, HI or molecular material. While a distant contribution to the soft X-ray background cannot be ruled out completely, especially given the complex origin for the NPS X-ray emission at ~ 0.15 keV (Iwan 1980), studies of polarized stars with known distances clearly prove that parts of the radio continuum Loop I are predominantly very local, <200 pc (Berdyugin et al. 2014; Santos et al. 2011). A study of Faraday tomography of the radio continuum adjacent to the NPS region determined that radio emission from the NPS is not Faraday depolarized, which also indicates the NPS ISMF is most likely within a few hundred parsecs

(Sun et al. 2015). The agreement between the properties of the S1 shell of Loop I (Wolleben 2007) and IBEX measurements of the LIC (Sect. 3.4) also indicates that Loop I is local.

3.3 The Local Bubble

The discovery of the soft X-ray background (SXRB, Bowyer et al. 1968) motivated measurements of the X-ray spectra at low energies, <0.25 keV, where the flat spectrum limited the amount of possible interstellar absorption of the X-ray photons (McCammon et al. 1983). The resulting "displacement model" required the X-rays to be produced inside a cavity in the neutral gas (Sanders et al. 1977; Williamson et al. 1974). The original interpretation of the SXRB data as tracing an evolved supernova remnant has been reviewed in Cox and Reynolds (1987); McCammon and Sanders (1990). Interpreting the physics of the hot gas has been surprisingly difficult because the local source of the hot plasma could not be identified. The supernova explosion that produced the Geminga pulsar was initially suggested to account for the soft X-ray emission (Gehrels et al. 2003), but Geminga was shown to originate near Orion instead (Frisch 1993; Pellizza et al. 2005; Smith et al. 1994). It is now known that the low-energy X-ray spectrum is contaminated by foreground emission from charge-exchange between solar wind plasma and interstellar neutrals (Koutroumpa et al. 2009).

It had been suggested by Cox and Smith (1974) that supernovae could form and maintain a mesh of interconnected tunnels of low-density high-temperature gas in the interstellar medium, producing structures similar to the Local Bubble. Frisch (1981) argued that the data indicated that the local interstellar medium had been processed by a shock front at least 2 Myr ago based on age limits set by the soft X-ray emissions and deep-sea sediments containing Be^{10} and suggested that it could be an extension of the Loop I or North Polar Spur seen in the Scorpius-Ophiucus region. In the opposite direction, one study predicts that the supernova forming the Antlia remnant exploded 1.20 Myr ago and 128 pc away at $\ell = 270.4$, $b = 19.2°$ (Tetzlaff et al. 2013). Smith and Cox (2001) have shown that multiple SNe within about 3 Myr can produce a bubble with conditions that resemble the Local Bubble. However, a model where a homogeneous local plasma at temperatures $\sim 10^6$ K accounts for all of the low energy X-ray emission has been elusive, as discussed in detail by Welsh and Shelton (2009).

No signs of a cluster of massive stars interior to the Local Bubble have been found. Using a kinematic analysis of the entire solar neighborhood within about 400 pc, Fuchs et al. (2006) have suggested that the youngest associations in the solar neighborhood entered the present bubble region about 10–15 Myr ago and that approximately 14–20 have exploded since then, a view consistent with the earlier studies of Maíz-Apellániz (2001). With the help of non-equilibrium ionization modeling, de Avillez and Breitschwerdt (2012) have constrained the evolution time since the last SN to be about 0.5–0.8 Myr. These parameters are in rough agreement with those derived from ^{60}Fe (see Sect. 4.1).

Charge exchange (CEX) between the solar wind ions and interstellar atoms has been suggested as at least a partial, if not complete, source for the diffuse X-ray background by Cravens et al. (2001). The origin of foreground contamination near 0.75 and 0.25 keV differ, with the former primarily due to CEX with solar wind oxygen atoms and the latter due to CEX with L-shell states for many species for which transition strengths are unknown (Kuntz et al. 2015). Foreground CEX predictions in the 0.75 keV band produce too hard of a spectrum to predict the CEX rates needed to discount an interstellar source of the SXRB (Frisch et al. 2009; Welsh and Shelton 2009). At lower energies, X-ray shadows are seen in the 0.094 keV Wisconsin band. The best models of simultaneous solar wind foreground and a thermal Local Bubble hot plasma indicate that the Local Bubble produces $26\% \pm 4\%$ of the 0.1–0.4 keV emissions (Smith et al. 2014). An alternative analysis finds solar wind charge exchange foreground levels of 43% to 76% of the SXRB produced by the Local Bubble in the 0.25 keV ROSAT band in the direction of the local cold Leo cloud (Snowden et al. 2015a,b). These results seem to reaffirm that the Local Bubble cavity is filled with a uniform hot gas but also indicate that more efforts to understand the foreground are needed.

The properties of the Local Bubble and the similarity to other (super)bubbles, coupled with the general observations of a three-phase interstellar medium with a hot phase consisting of low-density, high-temperature gas (Cox 2005), hint at a massive star and/or supernova origin. Other evidence within the Local Bubble also points towards a SN origin. Nehmé et al. (2008) and Gry et al. (2009) study the peculiar characteristics of a cometary-shaped infrared cirrus cloud towards the star HD 102065. The interpretation attributes the spatial structure in the cold phase, the high (and negative) velocities, the high abundance of atoms in excited states, a high level of ionization associated with the highest velocities, as well as the unusually high abundance of small dust particles, as all due to the interaction of the molecular cloud with a SN shock wave approximately 200,000 to 300,000 years ago.

3.4 Loop I and the Very Local Interstellar Medium

The physical characteristics of the nearest interstellar material, including the geometry of Loop I, local cloud kinematics, interstellar magnetic field, and gas-phase abundances, indicate an origin for the cluster of local interstellar clouds (CLIC) within ∼15 pc that is related to the Loop I superbubble. An alternate origin for the CLIC as a magnetic flux tube that detached from the Local Bubble walls (Cox and Helenius 2003) has not yet been tested against recent data. The CLIC contains kinematically defined interstellar clouds that are located mainly within 15 pc of the Sun (Fig. 4). The result that the Sun is in the rim of the Loop I superbubble rests on several arguments.

Geometrical considerations: Studies of the Loop I geometry consistently place the Sun in or close to the rim of the Loop I bubble if it is spherical. Models of radio Loop I and the NPS as a single shell yield a shell center at $\ell = 325°$, $b = 17.5°$,

Fig. 4 Nearby clouds:
Locations of the tenuous local
interstellar clouds within
~15 pc are shown projected
onto the galactic plane,
together with the cloud
motions through the LSR
(*blue arrows*, Frisch and
Schwadron 2014). Names are
shown for the clouds
(Redfield and Linsky 2008)
and several nearby stars. The
solar apex motion through the
LSR is marked with the
yellow arrow. The center of
the S1 shell is about 78 pc
beyond α Cen (Figure credit:
NASA, Adler Planetarium, P.
C. Frisch, S. Redfield)
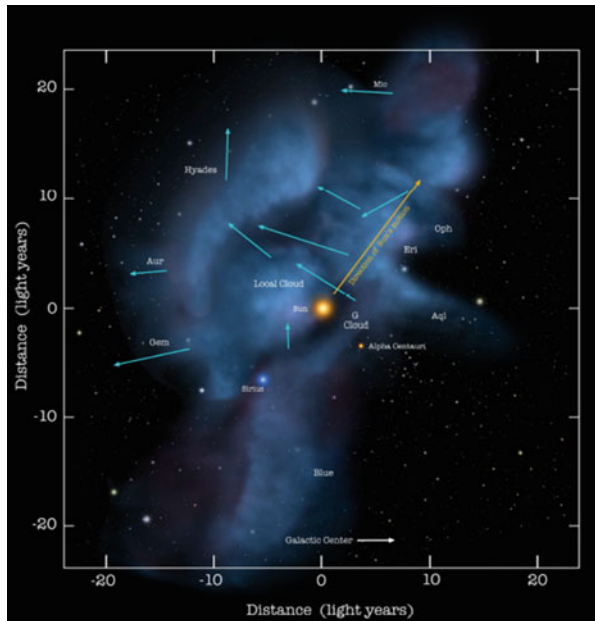
and 130 ± 75 pc with a diameter of 230 ± 135 pc (Berkhuijsen 1971; Berkhuijsen et al. 1971; Berkhuijsen 1973; Spoelstra 1972). Wolleben (2007) fits two separate spherical superbubble shells, S1 and S2, to the polarized Loop I radio continuum emission using a model of a spherical superbubble shell expanding in a uniform magnetic field (Frisch 2010, Figs. 1 and 3, left). The Sun is located in the rim of the S1 shell that is centered at $\ell \sim 346°$ and distance 78 ± 10 pc, with the distance comparable to the shell radius (62–101 pc). The HI 21-cm shell of Loop I is centered at $\ell = 320°$, $b = 5°$ and has a distance and radius of ~118 pc (Heiles 1998).

CLIC kinematics: The upwind direction of the bulk motion of the CLIC through the LSR is directed toward the center of Loop I, indicating that the Sun is in the Loop I shell that is still expanding at a velocity of $17.3 \, \mathrm{km \, s^{-1}}$ (Frisch et al. 2015). The kinematics of the low-density interstellar gas within 15 pc have been evaluated using two different assumptions: as a coherent flow of interstellar gas and dust through space (Bzowski 1988; Crutcher 1982; Frisch et al. 2002; Frisch and York 1986; Gry and Jenkins 2014) or as a group of separate cloudlets with different velocities (Frisch 2003; Frisch et al. 2002; Herbig 1968; Lallement et al. 1986; Redfield and Linsky 2008). Cloud velocities are found from interstellar absorption lines (e.g.,Herbig 1968; Rogerson et al. 1973). Velocities for the cloud around the heliosphere can also be estimated from in situ measurements of interstellar gas (e.g., Kubiak et al. 2016; Schwadron et al. 2015) and dust (Frisch et al. 1999; Kimura et al. 2003) that share similar velocities. The upwind direction of the interstellar wind coincides with the center of the S1 shell. An angle of $14° \pm 18°$ is found between the LSR

velocity of the bulk LSR velocity of the CLIC and the center of the S1 shell (Frisch 2010; Frisch et al. 2011; Frisch and Schwadron 2014). The flow of local ISM away from the Loop I region was discovered decades ago (Bzowski 1988; Crutcher 1982; Frisch 1979, 1981; Frisch and York 1986), and recent fits to different selections of interstellar absorption line data lead to similar results for the bulk flow, e.g., the vector directions in Gry and Jenkins (2014) and Frisch et al. (2002) differ by $11° \pm 17°$.

Perpendicular relation between interstellar magnetic field direction and LSR cloud velocities: Swept-up field lines near the equator of an expanding superbubble shell are perpendicular to the expansion velocity (Ferriere et al. 1991; Hanayama and Tomisaka 2006). Wolleben (2007) assumed such a configuration when evaluating the geometry of the S1 and S2 shells. This condition predicts cloud velocities that are perpendicular to the ISMF near the equatorial regions of the magnetic field. The bulk velocity of the CLIC through the LSR is perpendicular to the CLIC ISMF direction, and the LSR vector of the Local Interstellar Cloud (LIC) gas that surrounds the heliosphere is perpendicular to the LIC magnetic field direction. The angle between the bulk CLIC velocity and the interstellar magnetic field direction determined from polarized light from nearby stars is $80° \pm 8°$ (Frisch et al. 2015, 2011). The ISMF direction is obtained from the statistical analysis of polarized starlight, giving an ISMF pole toward $\ell = 36.2°$, $b = 49.0°$ ($\pm16°$) (Frisch et al. 2015), where the polarization is caused by the attenuation of starlight by a dichroic screen of foreground dust grains aligned with respect to the ISMF (Andersson et al. 2015). In the LIC, IBEX data give a magnetic field direction with a pole at $\ell = 34.8° \pm 4.3°$, $b = 56.6° \pm 1.2°$ (Frisch et al. 2015; Funsten et al. 2013), using as a direction proxy the center of the IBEX Ribbon of energetic neutral atoms (Funsten et al. 2013; McComas et al. 2009; Schwadron et al. 2009) which forms where the ISMF draping over the heliosphere is perpendicular to the sightline (e.g., McComas et al. 2014; Schwadron et al. 2009; Schwadron and McComas 2013). The LIC gas velocity is given by IBEX in situ measurements of interstellar neutrals (Frisch et al. 2015; McComas et al. 2015a; Möbius et al. 2009; Schwadron et al. 2013) and corresponds to a LIC LSR velocity of $17.2 \pm 1.9\,\mathrm{km\,s}^{-1}$ toward $\ell = 141.1° \pm 5.9°$, $b = 2.4° \pm 4.2°$. The enclosed angle α between the LIC ISMF and LSR velocity directions is perpendicular, $\alpha = 87.6° \pm 0.3°$ (Schwadron et al. 2014). The ISMF directions of the CLIC and LIC agree to within $7.6^{+14.9}_{-7.6}$ degrees (Frisch et al. 2015).

Local ISMF orders kinematics of local clouds: An alternate view of CLIC kinematics is provided by parsing the observed velocity components into individual cloudlets. A self-consistent analysis of separate cloud velocities has been developed by Redfield and Linsky (2008). Comparisons between the LSR velocities of these clouds (Frisch and Schwadron 2014) and the IBEX ISMF direction (Frisch et al. 2015; Funsten et al. 2013) reveal that the LSR cloud velocities are roughly proportional to the angle between the LSR cloud velocity vector and the ISMF direction (see Figure 12 of Frisch et al. 2015).

Abundance pattern of gas-phase elements: Clear evidence that the local ISM has been processed by passage through supernova shocks is provided by comparisons

between the abundance patterns of interstellar gas and solar abundances. Elements missing from the gas are due to the condensation of minerals onto dust grains (Ebel 2000). Frisch (1981) and Crutcher (1982) attributed the relatively high abundances of refractory elements in nearby interstellar gas to the erosion of grains by shocks originating in the Sco-Cen association. Early studies found that the gas-phase abundances of refractory elements increased with the cloud LSR velocity (Routly and Spitzer 1952; Sembach and Danks 1994; Spitzer 1976) because of the processing of interstellar dust in high-temperature shocks that erode the refractory component of the grains (e.g., Frisch et al. 2009; Jones et al. 1996; Siluk and Silk 1974; Slavin et al. 2015). Interstellar depletions for 243 sightlines (Jenkins 2009) have been characterized by considering the common parameter that describes the depletion pattern as a function of element and a second parameter that describes patterns between sightlines. Interstellar depletions increase with the total column density of HI but uncorrected ionization of the gas will lead to inaccurate larger values for gas-phase abundances of elements such as Fe^+ and Mg^+ with low first ionization potentials and therefore smaller depletions. The abundance patterns in the CLIC gas are similar to those of warm clouds (Welty et al. 1999) but vary between individual cloudlets (Redfield and Linsky 2008). The velocities of LIC gas (Schwadron et al. 2015) and LIC dust (from in situ measurements of interstellar dust inside of the heliosphere (Frisch et al. 1999; Kimura et al. 2003)) are in agreement indicating that the grain destruction must have occurred far in the past.

The best constrained interstellar cloud, the LIC, has an origin in a superbubble shell: The best understood interstellar cloud is the LIC that feeds interstellar gas (Frisch et al. 2009, 2011; McComas et al. 2015b) and dust (Altobelli et al. 2016; Frisch et al. 1999; Kimura et al. 2003; Sterken et al. 2015) into the heliosphere and is detected toward over 75 stars (Redfield and Linsky 2008). IBEX data permit the detailed study of the LIC at one spatial location; those data show that the LIC LSR velocity and LIC ISMF directions are perpendicular and the upwind direction of the LIC velocity is toward the center of Loop I (Frisch et al. 2015; McComas et al. 2015a; Schwadron et al. 2014). Abundances in the LIC have been corrected for ionization effects using self-consistent radiative transfer models (Slavin and Frisch 2008). Components of the models include a source of EUV photons to account for high ratios of HI/HeI found in pickup ion and anomalous cosmic ray data inside of the heliosphere (Cummings et al. 2002; Fisk et al. 1974; Gloeckler and Fisk 2007; Witte 2004), and toward nearby white dwarf stars (Frisch 1995; Wolff et al. 1999). Pickup ions and anomalous cosmic rays form from interstellar neutrals that survive penetration into the heliosphere (Bzowski et al. 2013) and are either directly sampled through in situ measurements (McComas et al. 2009, 2015a; Möbius et al. 2009; Park et al. 2014, 2015; Schwadron et al. 2013, 2016) or ionized through charge-exchange, photoionization, and other processes (Bzowski et al. 2013) to create the pickup ion population (Fisk et al. 1974; Gloeckler and Fisk 2007) or accelerated to become the anomalous cosmic ray population (Cummings et al. 2002). Using LIC data toward ε CMa and pickup ion and in situ heliospheric data, elemental abundances have been reconstructed for the LIC (Slavin 1989; Slavin and Frisch

2002, 2008). Predictions from these models include densities of $n_{HI} \sim 0.19$ cm^{-3}, $n(e) \sim 0.07$ cm^{-3}, ionization levels of hydrogen and helium $\sim 22\%$ and $\sim 39\%$, respectively, for a cloud temperature of 6300 K, the full destruction of carbonaceous grains in the LIC, and elevated gas-phase abundances for Fe and Mg that indicate silicate grains (Slavin and Frisch 2008). Solar abundances are also found for carbon in the low-density gas at intermediate and high velocities toward Orion (Welty et al. 1999, 2002). The LIC abundance pattern fits into the interstellar abundance patterns that depend on cloud velocity, which are nicely established for the low-velocity, intermediate velocity, and high-velocity clouds studied toward Orion where different clouds have been shocked differently (Welty et al. 1999, 2002).

3.5   The Orion-Eridanus Superbubble

The Orion region is the closest region that is actively forming high-mass stars. The activity of all the stars has combined to create the Orion-Eridanus bubble. At a distance of ~ 400 pc, it is a nearby expanding structure, explored over the entire wavelength range (Heiles et al. 1999), that serves as a testbed for superbubble theories. A recent paper Ochsendorf et al. (2015) has attempted to synthesize the previous data along with data collected from WISE and Planck to create a more complete model of the superbubble. The general picture emerging from their investigations is that the bubble is larger and more complex than was previously assumed (Fig. 5). It consists of a series of nested shells, the youngest of which, around the Orion Nebula Cluster, and is less than 1 Myr old. Some other smaller bubbles triggered by ongoing activity are found around λ Ori and the bubble GS206-17+13, most likely a stellar wind bubble approximately centered on the σ Ori cluster. In this model, Barnard's Loop is part of a complete bubble structure associated with a SNR that exploded about 0.3 Myr ago and then connected with the high-velocity gas detected in absorption studies toward this region. The expansion velocity of this structure is quite high, on the order of 100 km s^{-1}, again suggesting a recent origin. The outer shell of the Orion superbubble can be traced by observations of the intermediate velocity gas toward this region. In the west, some remnant of the neutral dense shell of the bubble can be seen, whereas toward the east, the shell is completely ionized. High temperature ($\geq 10^6$ K) X-ray emitting gas is seen toward the west, while the gas temperature in the eastern interior is two orders of magnitude lower.

The presence of various nested bubble structures suggests periods of episodic star formation in the Orion-Eridanus region. Instead of continuous input forming a single superbubble, each burst of star formation gave rise to different subgroups of stars that may locally ionize their environment, while stellar winds and the resulting SN explosions modify and tend to sweep up the surrounding medium into a bubble-like structure. The superbubble itself is probably 5–10 Myr old and was formed by a series of SNe that arose from stars in the Orion OB association. This model is supported further by the work of Pon et al. (2016), who have attempted to fit a Kompaneets model of a superbubble expanding in an exponential atmosphere to this
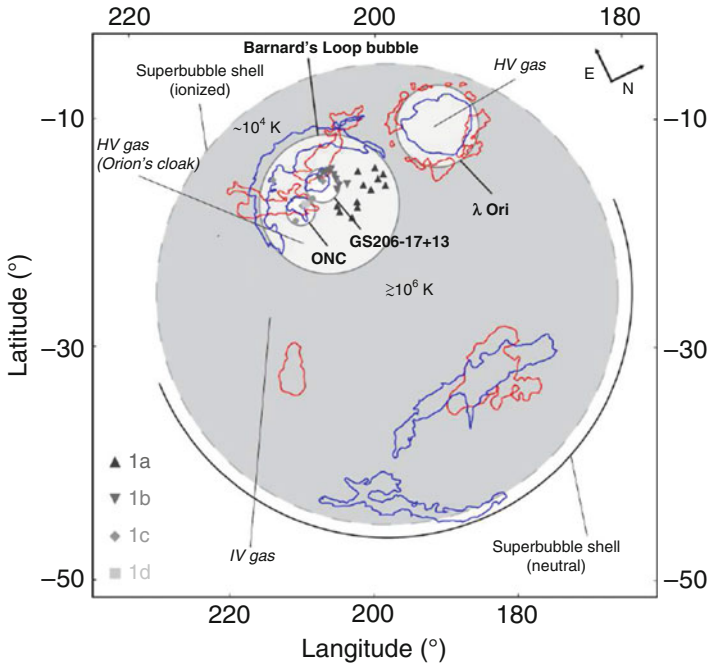
Fig. 5 Schematic of the Orion-Eridanus superbubble and several of its major components (Ochsendorf et al. 2015): the Orion-Eridanus superbubble is shown together with the structures that trace this bubble. A superbubble is formed from SNe in an old subpopulation of the Orion OB association and is traced by intermediate-velocity (IV) shocks (Welty et al. 1999, 2002). At lower galactic latitudes, the superbubble is surrounded by a shell of neutral swept-up material (*solid black line*) that is not apparent in the opposite direction. Nested younger and smaller shells are shown (*solid gray circles*) such as the famous Barnard's Loop feature (See Ochsendorf et al. (2015) for more information)

picture of the Orion-Eridanus bubble. They find morphologically consistent models with reasonable galactic scale heights of 80 pc, provided that the bubble is oriented with the Eridanus side (at lower latitudes) further from the Sun than the Orion side.

4   Isotopic and Abundance Indicators of SN Activity

4.1 ^{60}Fe Radioisotope Observations as Indicators of Nearby Supernovae

Measurements of ^{60}Fe in the terrestrial geological record provide an amazingly good indicator of encounters between supernovae ejecta and the heliosphere during the past several million years. ^{60}Fe is a radioactive isotope of iron with a half-life of 2.62 million years (Rugel et al. 2009). It is primarily produced in core collapse of massive stars, which typically eject 10^{-5} to 10^{-4} M$_\odot$ of ^{60}Fe (Limongi and

Chieffi 2003). A small amount may be produced during the s-process before core collapse or by asymptotic giant branch (AGB) stars. The important point is that there are no natural, terrestrial methods that produce ^{60}Fe; therefore, any terrestrial reservoirs of ^{60}Fe must be generally attributed to earlier deposition due to core-collapse supernovae (SNe) and can be considered as a signpost of the imprint of a nearby SN.

Using accelerator mass spectrometry, Knie et al. (1999) found evidence of enhanced concentrations of ^{60}Fe radioactivity in deep ocean ferromanganese crust in the South Pacific. Further and better measurements led them to suggest the presence of a significant increase in the ^{60}Fe concentrations about 2.8 Myr ago (Knie et al. 2004), suggesting the presence of a SN explosion within a few tens of parsecs from the solar system. Fields et al. (2005) combined the data with SNe nucleosynthesis models to refine the distance of a probable nearby SN to between 15 and 120 pc. Basu et al. (2007) posited an alternate theory that the ^{60}Fe was due to the presence of micrometeorites trapped by the crust rather than injection by a SN, but many of their arguments were refuted by Fitoussi et al. (2008).

Recent work seems to further substantiate the SN origin of ^{60}Fe. Wallner et al. (2016) found that the ^{60}Fe signal was global by finding evidence of ^{60}Fe deposition in deep-sea archives from the Indian, Pacific, and Atlantic oceans. Furthermore, they find interstellar influx ^{60}Fe onto earth via dust grains between 1.7 and 3.2 Myr ago, with a second signal 6.5–8.7 Myr ago. They argue that these signals suggest recent massive star ejections, presumably supernova explosions, in the solar neighborhood within about 100 pc. Breitschwerdt et al. (2016) have modeled the SN explosions that created the Local Bubble based on the evolution and supernova rates in star clusters forming the Sco-Oph groups. They suggest that the ^{60}Fe signal is mainly due to two SNe that occurred 1.5 and 2.3 Myr ago and between 90 and 100 pc distance from the solar system. The progenitor stars were about 9 $M_{\odot}$. An 8–10 $M_{\odot}$ SN occurring 2.8 Myr ago, with material arriving at the Earth 2.2 Myr ago, was also estimated by Fry et al. (2016).

Deep-ocean crusts are not the only evidence of ^{60}Fe concentrations. Fimiani et al. (2016) have confirmed earlier measurements (Cook et al. 2009; Fimiani et al. 2012) that showed an excess of ^{60}Fe concentrations in lunar cores, which presumably originated from the same events that led to the ^{60}Fe deposition in ocean crusts. By measuring the concentration of ^{53}Mn in the same samples, they suggest that the ^{60}Fe is likely of SN origin and that SN debris arrived on the moon about 2 Myr ago.

The Earth's microfossil record includes ^{60}Fe of biological origin. In 2013, Bishop et al. analyzed Pacific ocean sediment drill cores. They were able to extract ^{60}Fe from magnetofossils and quantify abundances using a mass spectrometer. Further analysis recently reported by Ludwig et al. (2016) confirms the direct detection of live ^{60}Fe atoms contained within secondary iron oxides, including magnetofossils, which are fossilized chains of magnetite crystals produced by magnetoactive bacteria. They suggest that the ^{60}Fe signal begins 2.6–2.8 Myr ago, peaks around 2.2 Myr earlier, and terminates around 1.7 Myr earlier, consistent with the time periods deduced from other data such as deep-ocean crusts and lunar samples.

The composition of galactic cosmic rays reveals their origin as well as provides hints to the cosmic ray acceleration mechanisms. Using the Cosmic Ray Isotope Spectrometer (CRIS) instrument on the Advanced Composition Explorer (ACE) spacecraft, ^{60}Fe has been detected in cosmic rays of a few hundred MeV/nucleon (Binns et al. 2016). The ^{60}Fe/^{56}Fe source ratio is $(7.5 \pm 2.9) \times 10^5$, which is consistent with that produced in massive stars. The detection of SN-produced ^{60}Fe in cosmic rays indicates that the time required for the acceleration and transport of the cosmic rays to earth cannot exceed the half-life of ^{60}Fe of 2.62 Myr. Consequently, the distance from the source should be comparable to the distance that cosmic rays can diffuse over this time period, which they estimate to be less than 1 kpc. This is consistent with the existence of a SN within a kpc that exploded during the last 2.6 Myr.

4.2   Isotopes and the OB Association Origin of Galactic Cosmic Rays

Elemental abundances of galactic cosmic rays (GCRs) reveal both the origin and the acceleration mechanism of the GCRs. The largest differences between the isotopic composition of the GCRs and solar system values are found for the ratios ^{22}Ne/^{20}Ne, ^{12}C/^{16}O, and ^{58}Fe/^{56}Fe. The ratio ^{22}Ne/^{20}Ne in GCRs is a factor of 5.3 ± 0.3 larger than the value in the solar wind (Binns et al. 2005). Measurements of ^{22}Ne/^{20}Ne in the anomalous cosmic ray population (ACR) at lower energies, which form from interstellar neutrals that become charged while interacting with heliospheric plasma, show ratios consistent with solar values (Leske 2000). The enhanced ratio ^{22}Ne/^{20}Ne in GCRs suggests a source that includes contributions from the ejecta of massive stars. Binns et al. (2005) have shown that the ratio can be explained as resulting from a mixture of $\approx$20% massive star ejecta and wind material with $\sim$80% interstellar medium. In fact, they further show that such an admixture could explain a range of isotope and element ratios for $Z \leq 28$ nuclei. Newer measurements (Murphy et al. 2016) of abundances with $Z \geq 26$ are consistent with this and indicate that GCRs have formed from a mixture of 19% ejecta from massive stars and 81% interstellar material with solar system composition. This means that the stellar winds and/or supernova has mixed with only about four times their ejected mass, which implies that the stellar source must not be mixing with too much interstellar material, suggesting the nearby presence of massive stars and/or supernovae.

Another isotopic constraint from GCRs is the lack of ^{59}Ni in cosmic rays. ^{59}Ni has a half-life of 76,000 years before it decays to ^{59}Co by electron capture. Once it is accelerated to high energy, the ^{59}Ni is stripped of electrons and therefore cannot decay. Data from the CRIS experiment show a lack of ^{59}Ni in GCRs, indicating that the ^{59}Ni has decayed from the amount one would expect from a SN explosion (Wiedenbeck et al. 1999). Therefore Wiedenbeck et al. (1999) suggest that acceleration of the material took place at least 76,000 years after it was ejected. Thus while the ^{22}Ne/^{20}Ne ratio suggests that acceleration could not have taken

place more than a few million years after the wind material was ejected (to avoid mixing too much interstellar medium material), the ^{59}Ni measurement shows that it must be at least 0.1 Myr after the SN explosion. It is possible that acceleration in superbubbles can satisfy both these constraints. However, it should be noted that a recent analysis by Neronov and Meynet (2016), taking the yield of ^{59}Ni from updated massive star models for stars up to 120 $M_\odot$, suggests a low ^{59}Ni yield compared to ^{59}Co, consistent with the CRIS experiments, which may remove the need for this constraint.

Balloon-born TIGER measurements of heavy GCRs $_{26}$Fe through $_{40}$Zi (Murphy et al. 2016; Rauch et al. 2009) show that the abundances of $_{26}$Fe through $_{40}$Zi in the galactic cosmic ray population adhere to a pattern where the refractory elements in the GCR population are enhanced over volatile elements. Refractory elements in GCRs with energies of hundreds of MeV per nucleon to GeV per nucleon show a preferential acceleration of a factor of four over the acceleration of volatiles (Murphy et al. 2016). Epstein (1980) was one of the first to explain the high abundance of refractory elements in cosmic rays, by suggesting that they were preferentially accelerated. Bibring and Cesarsky (1981) indicated that SN shocks can pick up particles from a suprathermal population produced by the destruction of dust grains. Ellison et al. (1997) produced the first detailed model explaining GCR abundances and isotopic ratios using interstellar grains that are accelerated to modest energies by SN shock waves. Grain destruction in the shock layer results from the thermal sputtering of particles from grain surfaces due to gas-grain collisions and grain shattering and vaporization during grain-grain collisions (Barlow and Silk 1977; Draine and Salpeter 1979; Jones et al. 1994, 1996). Refractory elements show a well-known resilience against destruction. High-condensation temperatures lead to refractory elements being injected into the shock at higher energies than volatiles, giving rise to the preferential acceleration of refractory elements in contrast to the volatiles that are accelerated in accordance with their mass-to-charge ratio (Ellison et al. 1997).

4.3 ^{26}Al as a Tracer of Massive Stars

In 1999, Knödlseder showed from an analysis of Comptel data that the 1.8 MeV gamma-ray line was closely correlated with the 53 GHz free-free emission in the Galaxy. 1.8 MeV gamma-rays are emitted during the radioactive decay of ^{26}Al, which has a half-life of about 0.7 Myr. The free-free emission arises from the ionized interstellar medium. He argued that this could be understood if massive stars are the source of ^{26}Al. Knödlseder et al. (1999) showed that the correlation was also strong with other tracers of the young stellar population, which confirmed that the source of ^{26}Al was massive stars and supernovae.

Using spatial maps from the Comptel observatory to identify isolated regions of γ-ray emission and the INTEGRAL γ-ray spectrometer to identify the γ-ray velocities, Diehl et al. (2010) identified a γ-ray source expanding toward the Sun at 137 ± 75 km s^{-1} from a 10°-radius region centered on the Upper-Scorpius (US)

subgroup of the Sco-Cen association. Given the 0.717 Myr half-life of ^{26}Al, this implies that the massive stars were born less than 10 Myr ago, thus indicating recent star formation. De Geus (1992) suggested that the proto-US cloud was compressed by an expanding shell from the Upper Centaurus-Lupus association $\sim$4 Myr ago, igniting star formation. Since the velocity of the γ-ray source exceeds the $\sim$10 km s^{-1} velocity of the HI shell around the US subgroup, Diehl et al. (2010) have adopted the scenario where the high-velocity gas is stellar ejecta streaming into an adjacent preexisting cavity and that deceleration occurred as the gas collided with the preexisting walls of the bubble (Diehl et al. 2010). The young star clusters in a spiral arm will feed ^{26}Al ejecta into preexisting HI supershell cavities that were left over from earlier star formation during passage of the previous spiral arm density wave (Krause et al. 2015).

5   Impact of Supernova on Heliosphere

Supernovae impact the heliosphere through the direct encounter of the heliosphere with the SN blast wave or ejecta or modification of the ISM properties at the heliosphere. As discussed above, the Sun is traveling through the shell of the Loop I superbubble that resulted from stellar evolution in the Sco-Cen OB2 association. It was recognized long ago that extreme variations in the physical properties of interstellar material interacting with the solar system would probably affect the terrestrial climate (Clark et al. 1977; Frisch 1993, 2006; Hoyle and Lyttleton 1939; Müller et al. 2006; Scherer et al. 2006; Shapley 1921). These effects are mediated by the interaction between the heliosphere and interstellar medium (Frisch 1993; Holzer 1989; Müller et al. 2006; Scherer et al. 2006; Zank 2015; Zank and Frisch 1999). The 18 km s^{-1} motion of the solar system through the LSR and the 7–47 km s^{-1} LSR velocities of nearby interstellar clouds (Frisch and Schwadron 2014) lead to variations in the heliospheric boundary conditions over geological timescales of order $\leq$30 kyr (Frisch and Mueller 2011). Implications of our changing galactic environment are discussed in Scherer et al. (2006) and Frisch (2006).

The heliosphere configuration is governed by the relative pressures of the solar wind and interstellar material, including the dynamic ram pressure that increases nonlinearly with the interaction velocity $\sim V^2$, and by interstellar ionizations since excluded ions and penetrating neutrals interact differently (Holzer 1989; Zank 2015). Even a moderate increase in the relative velocities of the Sun and surrounding interstellar cloud from the present 25.4 km s^{-1} LIC velocity (McComas et al. 2015a; Schwadron et al. 2015) to 45 km s^{-1} (e.g. the cloud named "Vela" in Redfield and Linsky 2008) leads to a decrease of the heliopause distance by 34% from 104 to 69 AU (Müller et al. 2006). Interactions between the heliosphere and an evolving superbubble at different velocities lead to different configurations for the heliosphere. Variations in the heliosphere-interstellar interactions also arise from
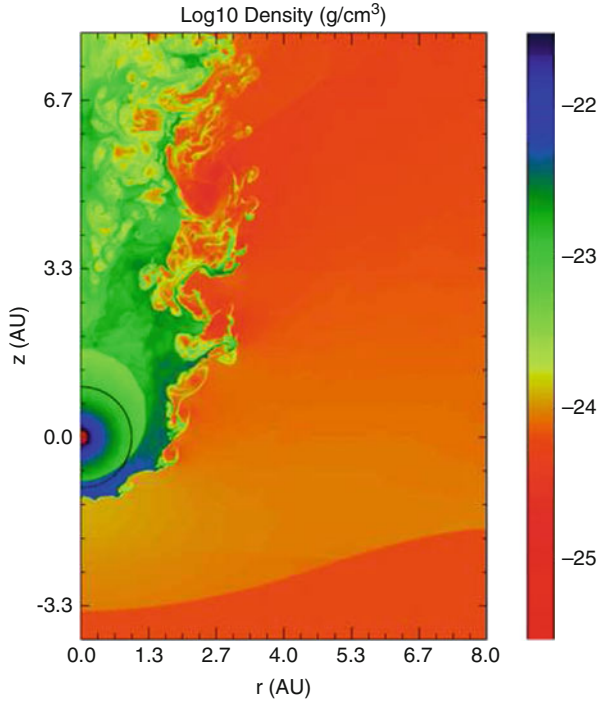
Fig. 6 One scenario showing the impact of a SNe blast wave on the heliosphere. A map of the logarithmic density of the heliosphere is shown after interaction with the shock from a supernova explosion 10 pc away for an explosion occurring in a tenuous unmagnetized low-density cloud similar to the LIC. The Sun is located at the origin. Two shocks result, the innermost shock forms where the solar wind decelerates from a supersonic to a subsonic plasma, and the outer shock, the heliospheric bow shock, occurs where the blast wave becomes subsonic. The interface between the two fluids is marked by Kelvin-Helmholtz instabilities. In this model, the SNR dominates the solar wind at 1 AU (See Fields et al. 2008 for additional information)

variations in the solar magnetic activity cycle (e.g., Pogorelov et al. 2013; Washimi and Tanaka 1999).

The extreme example of the influence of our galaxy on the heliosphere would arise from the explosion of a supernova close to the Sun (Fig. 6). The ionizing photons from the massive star preceding a core-collapse supernova would, if close to the Sun, create a fully ionized environment for the heliosphere. The supernova explosion would first be noticed by an intense flux of UV/X-ray photons from the SN explosion itself that could ionize and heat the cloud around the heliosphere. A counterintuitive result is that the flux of galactic cosmic rays at the Earth will increase for immersion of the heliosphere in a fully ionized plasma (Fig. 7). Penetrating interstellar neutrals become ionized through charge-exchange, photoionization, and other processes (Bzowski et al. 2013) to create pickup ions that become accelerated to form anomalous cosmic rays (Fisk et al. 1974). The pickup
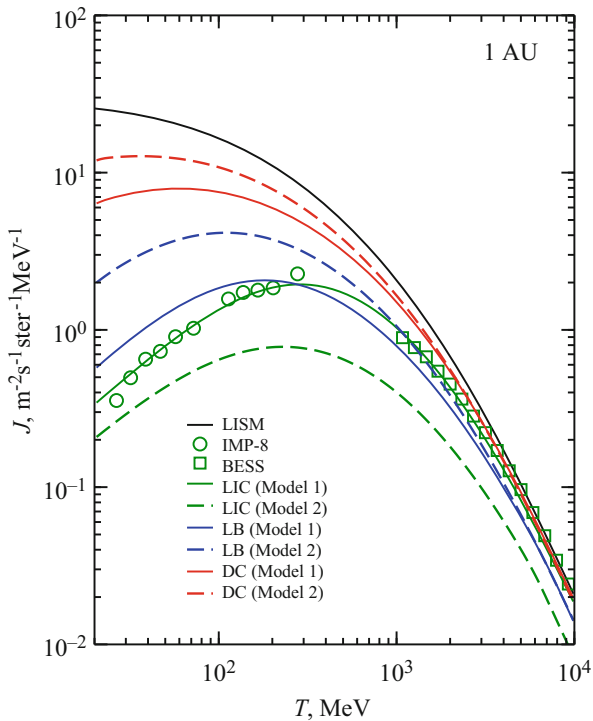
Fig. 7 Galactic cosmic ray fluxes at the Earth for different solar environments. Higher GCR fluxes are found at the Earth when the Sun is immersed in a fully ionized hot plasma (*blue lines*) compared to for today's immersion of the Sun in the LIC (*green lines*). This effect arises from the charge-exchange between the interstellar neutrals and the solar wind that increases turbulence and the modulation of the GCR component through mass loading (See Müller et al. 2009 for more information)

ions that are trapped on the solar wind magnetic field lines mass load the wind and increase turbulence that impedes the propagation of galactic cosmic rays to the inner heliosphere. Figure 7 shows that GCR fluxes in the inner heliosphere could increase by an order of magnitude if the surrounding interstellar cloud became fully ionized by a nearby supernova.

A blast wave from a nearby supernova would compress the heliosphere. Heliosphere multifluid models predict an encounter with a decelerated superbubble shell that, at a velocity $100 \, \mathrm{km \, s^{-1}}$ relative to the heliosphere, would shrink the heliopause to ∼14 AU for a warm tenuous cloud (8,000 K, $n \sim 0.8 \, \mathrm{cm^{-3}}$, Müller et al. 2006). Numerical simulations show that a blast wave of thousands of $\mathrm{km \, s^{-1}}$ would sweep away the heliosphere, possibly leaving the Earth directly immersed in the supernova remnant. Fields et al. (2008) simulated a scenario for the heliosphere responding to a supernova that is located 8 pc away (Fig. 6). The interface between the solar wind and remnant plasma becomes highly unstable due to Kelvin-Helmholtz instabilities. These particular simulations do not explore a medium modified by the winds of the

progenitor star (e.g., Dwarkadas 2005, 2007; Garcia-Segura et al. 1996a), which could alter the scenario.

The proximity of active OB stars to the Sun could lead to an excess of photons at the time of shock breakout that would result in a potentially significant influence on the physical conditions of the interstellar medium that shapes the heliosphere. There is no a priori basis for assuming a constant radiation field at the Earth over the past $\sim$1 Myr. Slavin and Frisch (1996) have modeled the photon burst created by the supernova parent of the young Vela pulsar, $<30,000$ years old and located at edge of the low-density Local Bubble region in the near side of the Gum Nebula, and suggested that the supernova may have contributed to the ionization of the interstellar cloud around the heliosphere. Recombination times for LIC-like gas at densities $0.1\,\mathrm{cm}^{-3}$ are $\sim$650,000 years and longer if the gas is hotter. Possible sources of the ionizing radiation include γ-rays and the breakout of the supernova shock from the stellar atmosphere. Brakenridge (1981) concluded that radiation from a nearby supernova may have left isotopic signatures in the ^{14}C terrestrial record and that the Vela supernova may explain a ^{14}C anomaly 15,000 years ago.

6   Conclusions

The interstellar medium of the solar neighborhood within $\sim$500 pc has been shaped by the massive stars assigned to Gould's Belt in earlier studies. The nearest region of star formation is in the Scorpius-Centaurus association where multiple supernovae have erupted during the past 15 Myr. Winds and supernova in these regions create bubbles and superbubbles that remix the interstellar medium over spatial scales of 500 pc. These bubbles are detected as filaments and loops of synchrotron emission arising from the compressed interstellar magnetic fields in the bubble walls and/or shells of HI gas swept up by the expanding bubbles. Two examples are the Loop I superbubble, which has expanded to the solar location, and the more distant Orion-Eridanus superbubble. The cluster of local interstellar clouds, as well as the ISM flowing through the heliosphere, display signatures of an origin inside of the rim of the Loop I superbubble, including the interstellar magnetic field direction and cloud velocities through the LSR. Cosmic ray isotopes trace the mixing of local interstellar material with the interstellar medium. The discovery of short-lived radioisotopes in the geologic record indicates that the Earth has received material from supernovae occurring within the past $\sim$2 Myr. Heliosphere models show that the heliosphere is a sensitive barometer for interstellar pressures and would react dramatically to the explosion of a nearby supernova. A diversity of astrophysical and geological data are converging to allow new insights into the origin of interstellar material around the Sun and to expand our perspective to include the relation between the heliosphere and the Milky Way galaxy.

7   Cross-References

▶ Dust and Molecular Formation in Supernovae
▶ Dynamical Evolution and Radiative Processes of Supernova Remnants
▶ Gould's Belt: Local Large-Scale Structure in the Milky Way
▶ High-Energy Cosmic Rays from Supernovae
▶ Impact of Supernovae on the Interstellar Medium and the Heliosphere
▶ Infrared Emission from Supernova Remnants: Formation and Destruction of Dust
▶ Isotope Variations in the Solar System: Supernova Fingerprints
▶ Stardust from Supernovae and Its Isotopes
▶ Structures in the Interstellar Medium Caused by Supernovae: The Local Bubble
▶ Supernovae from Massive Stars
▶ Supernova Remnants as Clues to Their Progenitors
▶ The Supernova – Supernova Remnant Connection
▶ X-Ray Emission Properties of Supernova Remnants

References

Alfaro EJ, Cabrera-Cano J, Delgado AJ (1991) Topography of the Galactic disk – Z-structure and large-scale star formation. ApJ 378:106. doi:10.1086/170410

Alfaro EJ, Elias F, Cabrera-Caño J (2009) Star-formation modes in the solar neighborhood. Ap&SS 324:141. doi:10.1007/s10509-009-0119-2

Altobelli N, Postberg F et al (2016) Flux and composition of interstellar dust at Saturn from Cassini's cosmic dust analyzer. Science 352:312–318, eid 6283. doi:10.1126/science.aac6397

Andersson GB, Lazarian A, Vaillancourt EJ (2015) Interstellar dust grain alignment. Ann Rev Astron Astrophys 53:501–539. doi:10.1146/annurev-astro-082214-122414

Basu S, Stuart MF, Schnabel C, Klemm V (2007) Galactic-cosmic-ray-produced He3 in a ferromanganese crust: any supernova Fe60 excess on earth? Phys Rev Lett 98(14):141103. doi:10.1103/PhysRevLett.98.141103

Barlow MJ, Silk J (1977) Absorption, heavy elements, interstellar matter, shock wave propagation, sputtering, supernova remnants, abundance, granular materials, propagation velocity, shock fronts. ApJ Lett 211:L83–L87. doi:10.1086/182346

Berdyugin A, Piirola V, Teerikorpi P (2014) Interstellar polarization at high galactic latitudes from distant stars. VIII. Patterns related to the local dust and gas shells from observations of ˜3600 stars. A&A 561:A24. doi:10.1051/0004-6361/201322604

Berkhuijsen ME (1971) A survey of the continuum radiation at 820 MHz between declinations -7deg and +85deg. A study of the galactic radiation and the degree of polarization with special reference to the Loops and Spurs. A&A 14:359

Berkhuijsen EM, Haslam CGT, Salter CJ (1971) Are the galactic loops supernova remnants? A&A 14:252–262

Berkhuijsen ME (1973) Galactic continuum loops and the diameter-surface brightness relation for supernova remnants. A&A 24:143–147

Bibring JP, Cesarsky CJ (1981) Interstellar grains as seeds for galactic cosmic rays. Int Cosm Ray Conf 2:289–291

Binns RW, Wiedenbeck EM, Arnould M, Cummings CA, George SJ, Goriely S, Israel HM, Leske AR, Mewaldt AR, Meynet G, Scott LM, Stone CE, von Rosenvinge TT (2005) Cosmic-ray neon, Wolf-Rayet Stars, and the superbubble origin of galactic cosmic rays. ApJ 634:351–364. doi:10.1086/496959

Binns RW, Israel HM, Christian RE, Cummings CA, de Nolfo GA, Lave AK, Leske AR, Mewaldt AR, Stone CE, von Rosenvinge TT, Wiedenbeck EM (2016) Observation of the ^{60}Fe nucleosynthesis-clock isotope in galactic cosmic rays. Science 352:677–680. doi:10.1126/science.aad6004

Bishop S, Ludwig P, Egli R, Chernenko V, Frederichs T, Merchel S, Rugel G (2013) Search for supernova ˆ60Fe in the Earth's fossil record. APS April Meeting Abstracts (2013)

Blaauw A (1964) The O associations in the solar neighborhood. Ann Rev Astron Astrophys 2:213. doi:10.1146/annurev.aa.02.090164.001241

Bobylev VV (2014) The Gould Belt. Astrophysics 57:583–604. doi:10.1007/s10511-014-9360-7

Bobylev VV, Bajkova AT (2014) The Gould Belt, the de Vaucouleurs-Dolidze belt, and the Orion arm. Astron Lett 40:783–792. doi:10.1134/S1063773714120020

Bowyer SC, Field BG, Mack FJ (1968) Detection of an anisotropic soft X-ray background flux. Nature 217:32

Brakenridge GR (1981) Terrestrial paleoenvironmental effects of a late quaternary-age supernova. Icarus 46:81–93

Breitschwerdt D, Feige J, Schulreich MM, Avillez MAD, Dettbarn C, Fuchs B (2016) The locations of recent supernovae near the Sun from modelling ^{60}Fe transport. Nature 532:73–76. doi:10.1038/nature17424

Bzowski M (1988) Local interstellar wind velocity from Doppler shifts of interstellar matter lines. Acta Astron 38:443–453

Bzowski M, Sokół JM, Kubiak AM, Kucharek H (2013) Modulation of neutral interstellar He, Ne, O in the heliosphere. Survival probabilities and abundances at IBEX. A&A 557:A50. doi:10.1051/0004-6361/201321700

Castor J, McCray R, Weaver R (1975) Interstellar bubbles. ApJ Lett 200:L107–L110. doi:10.1086/181908

Chu HY, Gruendl AR, Guerrero AM (2003a) An inside-out view of bubbles. In: Arthur J, Henney WJ (eds) Revista Mexicana de Astronomia y Astrofisica. Revista Mexicana de Astronomia y Astrofisica Conference Series, vols 27, 15. Universidad Nacional Autonoma de Mexico, Mexico City, pp 62–67

Chu HY, Guerrero AM, Gruendl AR, García-Segura G, Wendker HJ (2003b) Hot gas in the circumstellar bubble S308. ApJ 599:1189–1195. doi:10.1086/379607

Clark DH, McCrea WH, Stephenson FR (1977) Frequency of nearby supernovae and climatic and biological catastrophes. Nature 265:318-+

Cook LD, Berger E, Faestermann T, Herzog FG, Knie K, Korschinek G, Poutivtsev M, Rugel G, Serefiddin F (2009) 60Fe, 10Be, and 26Al in Lunar Cores 12025/8 and 60006/7: search for a nearby supernova. In: Lunar and planetary science conference. Lunar and Planetary Institute Technical Report, vol 40, p 1129

Cox PD (2005) The three-phase interstellar medium revisited. Ann Rev Astron Astrophys 43: 337–385. doi:10.1146/annurev.astro.43.072103.150615

Cox PD, Helenius L (2003) Flux-tube dynamics and model for the origin of the local fluff. ApJ 583:205–228

Cox PD, Reynolds JR (1987) The local interstellar medium. Ann Rev Astron Astrophys 25: 303–344. doi:10.1146/annurev.aa.25.090187.001511

Cox PD, Smith WB (1974) Large-scale effects of supernova remnants on the galaxy: generation and maintenance of a hot network of tunnels. ApJ Lett 189:L105. doi:10.1086/181476

Cravens ET, Robertson PI, Snowden LS (2001) Temporal variations of geocoronal and heliospheric X-ray emission associated with the solar wind interaction with neutrals. J Geophys Res 106:24883–24892

Crawford AI (1991) High resolution observations of interstellar NA I and CA II towards the Scorpio-Centaurus Association. A&A 247:183–201

Crutcher MR (1982) The local interstellar medium. ApJ 254:82–87

Cummings CA, Stone CE, Steenberg DC (2002) Composition of anomalous cosmic rays and other heliospheric ions. ApJ 578:194–210

Davies DR (1964) The galactic Spur. MNRAS 128:173. doi:10.1093/mnras/128.2.173

de Avillez MA, Breitschwerdt D (2012) Non-equilibrium ionization modeling of the Local Bubble. I. Tracing Civ, Nv, and Ovi ions. A&A 539:L1. doi:10.1051/0004-6361/201117172

de Geus EJ (1991) Interaction of massive stars with the interstellar medium. In: Janes K (eds) The formation and evolution of star clusters. Astronomical Society of the Pacific conference series, vol 13. Astronomical Society of the Pacific, San Francisco, pp 40–54

de Geus EJ (1992) Interactions of stars and interstellar matter in Scorpio Centaurus. A&A 262:258

Diehl R, Lang MG, Martin P, Ohlendorf H, Preibisch T, Voss R, Jean P, Roques JP, von Ballmoos P, Wang W (2010) Radioactive ^{26}Al from the scorpius-centaurus association. A&A 522:A51. doi:10.1051/0004-6361/201014302

Draine BT, Salpeter EE (1979) Destruction mechanisms for interstellar dust. ApJ 231:438–455

Dwarkadas VV (2005) The evolution of supernovae in circumstellar wind-blown bubbles. I. Introduction and one-dimensional calculations. ApJ 630:892–910. doi:10.1086/432109

Dwarkadas VV (2007) The evolution of supernovae in circumstellar wind bubbles. II. Case of a Wolf-Rayet Star. ApJ 667:226–247. doi:10.1086/520670

Dwarkadas VV, Rosenberg LD (2013) Simulated X-ray spectra from ionized wind-blown nebulae around massive stars. High Energy Density Phys 9:226–230. doi:10.1016/j.hedp.2012.12.003

Dwarkadas VV, Rosenberg D (2015) X-ray emission from ionized wind-bubbles around Wolf-Rayet Stars. In: Hamann W-R, Sander A, Todt H (eds) Wolf-Rayet Stars: proceedings of an international workshop held in Potsdam, 1–5 June 2015. Universitätsverlag Potsdam, pp 329–332

Ebel SD (2000) Variations on solar condensation: Sources of interstellar dust nuclei. J Geophys Res 105:10363–10370

Egger JR, Aschenbach B (1995) Interaction of the Loop I supershell with the local hot bubble. A&A 294:L25–L28

Elias F, Alfaro EJ, Cabrera-Caño J (2009) Hierarchical star formation: stars and stellar clusters in the Gould Belt. MNRAS 397:2–13. doi:10.1111/j.1365-2966.2009.14465.x

Ellison DC, Drury LO, Meyer J (1997) Galactic cosmic rays from supernova remnants. II. Shock acceleration of gas and dust. ApJ 487:197

Epstein RI (1980) The acceleration of interstellar grains and the composition of the cosmic rays. MNRAS 193:723–729. doi:10.1093/mnras/193.4.723

Ferriere MK, Mac Low M, Zweibel GE (1991) Expansion of a superbubble in a uniform magnetic field. ApJ 375:239–253

Fields DB, Hochmuth AK, Ellis J (2005) Deep-ocean crusts as telescopes: using live radioisotopes to probe supernova nucleosynthesis. ApJ 621:902–927

Fields BD, Athanassiadou T, Johnson SR (2008) Supernova collisions with the heliosphere. ApJ 678:549–562. doi:10.1086/523622

Fimiani L, Cook LD, Faestermann T, Gomez Guzman JM, Hain K, Herzog FG, Korschinek G, Ligon B, Ludwig P, Park J, Reedy RC, Rugel G (2012) Sources of live ^{60}Fe, ^{10}Be, and ^{26}Al in Lunar Core 12025, Core 15008, Skim Sample 69921, Scoop Sample 69941, and Under-Boulder Sample 69961. In: Lunar and planetary science conference. Lunar and Planetary Institute Technical Report, vol 43, p 1279

Fimiani L, Cook LD, Faestermann T, Gómez-Guzmán JM, Hain K, Herzog G, Knie K, Korschinek G, Ludwig P, Park J, Reedy CR, Rugel G (2016) Interstellar Fe 60 on the surface of the Moon. Phys Rev Lett 116(15):151104. doi:10.1103/PhysRevLett.116.151104

Fisk LA, Kozlovsky B, Ramaty R (1974) An interpretation of the observed oxygen and nitrogen enhancements in low energy cosmic rays. ApJ 190:L35–L38

Fitoussi C, Raisbeck MG, Knie K, Korschinek G, Faestermann T, Goriely S, Lunney D, Poutivtsev M, Rugel G, Waelbroeck C, Wallner A (2008) Search for supernova-produced Fe60 in a marine sediment. Phys Rev Lett 101(12):121101. doi:10.1103/PhysRevLett.101.121101

Florinski V, Zank GP (2006) The galactic cosmic ray intensity in the heliosphere in response to variable interstellar environments. In: Frisch PC (ed) Solar journey: the significance of our galactic environment for the heliosphere and earth. Springer, Dordrecht, pp 281–316

Freyer T, Hensler G, Yorke WH (2003) Massive stars and the energy balance of the interstellar medium. I. The impact of an isolated 60 M_{solar} Star. ApJ 594:888–910. doi:10.1086/376937

Freyer T, Hensler G, Yorke WH (2006) Massive stars and the energy balance of the interstellar medium. II. The 35 M_{solar} Star and a Solution to the "Missing Wind Problem". ApJ 638: 262–280. doi:10.1086/498734

Frisch PC (1979) The interstellar material in front of Chi Ophiuchi. I – optical observations. ApJ 227:474–482

Frisch PC (1981) The nearby interstellar medium. Nature 293:377–379. doi:10.1038/293377a0

Frisch PC (1993) Whence Geminga. Nature 364:395

Frisch PC (1993) ApJ G-star astropauses – a test for interstellar pressure. 407:198–206

Frisch PC (1995) Characteristics of nearby interstellar matter. Space Sci Rev 72:499–592

Frisch PC (2003) Local interstellar matter: the apex cloud. ApJ 593:868–873

Frisch PC (2006) Solar journey: the significance of our galactic environment for the heliosphere and earth. Springer, Dordrecht

Frisch PC (2010) The S1 shell and interstellar magnetic field and gas near the heliosphere. ApJ 714:1679–1688. doi:10.1088/0004-637X/714/2/1679

Frisch PC, Andersson BG, Berdyugin A, Piirola V, Funsten HO, Magalhaes AM, Seriacopi DB, McComas DJ, Schwadron NA, Slavin JD, Wiktorowicz SJ (2015) Evidence for an interstellar dust filament in the outer heliosheath. ApJ 805:60. doi:10.1088/0004-637X/805/1/60

Frisch PC, Berdyugin A, Piirola V, Magalhaes AM, Seriacopi D, Ferrari T, Santos FP, Schwadron N, Funsten HO, McComas DJ, Heiles C (2016, in press) Tracing the structure of the interstellar magnetic field around the heliosphere using polarized starlight. AGU Fall Meet Abstr SHA312544

Frisch PC, Bzowski M, Grün E, Izmodenov V, Krüger H, Linsky JL, McComas DJ, Möbius E, Redfield S, Schwadron N, Shelton RR, Slavin JD, Wood BE (2009) The galactic environment of the Sun: interstellar material inside and outside of the heliosphere. Space Sci Rev 146: 235–273

Frisch PC, Dorschner MJ, Geiss J, Greenberg MJ, Grün E, Landgraf M, Hoppe P, Jones PA, Krätschmer W, Linde JT, Morfill EG, Reach W, Slavin DJ, Svestka J, Witt NA, Zank GP (1999) Dust in the local interstellar wind. ApJ 525:492–516

Frisch PC, Grodnicki L, Welty ED (2002) The velocity distribution of the nearest interstellar gas. ApJ 574:834–846

Frisch PC, Mueller HR (2011) Time-variability in the interstellar boundary conditions of the heliosphere: effect of the solar journey on the galactic cosmic ray flux at earth. Space Sci Rev pp 130–+. doi:10.1007/s11214-011-9776-x

Frisch PC, Redfield S, Slavin J (2011) The interstellar medium surrounding the Sun. Ann Rev Astron Astrophys 49:237–279

Frisch PC, Schwadron AN (2014) Large-scale Interstellar Structure and the Heliosphere. In: Hu Q, Zank GP (eds) Outstanding problems in heliophysics: from coronal heating to the edge of the heliosphere. Astron Soc Pac Conf Ser 484:42

Frisch P, York GD (1986) Interstellar clouds near the Sun. In: Smoluchowski R, Bahcall J, Matthews M (eds) The galaxy and the solar system. University of Arizona Press, Tucson, pp 83–100

Fry JB, Fields DB, Ellis RJ (2016) Radioactive Iron Rain: Transporting ^{60}Fe in Supernova Dust to the Ocean Floor. ApJ 827:48. doi:10.3847/0004-637X/827/1/48

Fuchs B, Breitschwerdt D, de Avillez MA, Dettbarn C, Flynn C (2006) The search for the origin of the local bubble redivivus. MNRAS 373:993–1003. doi:10.1111/j.1365-2966.2006.11044.x

Funsten HO, DeMajistre R, Frisch PC, Heerikhuijsen J, Higdon DM, Janzen P, Larsen B, Livadiotis G, McComas DJ, Möbius E, Reese C, Reisenfeld DB, Schwadron NA, Zirnstein EJ (2013) Circularity of the IBEX ribbon of enhanced energetic neutral atom (ENA) fluxes. ApJ 776:30

Garcia-Segura G, Mac Low MM, Langer N (1996) The dynamical evolution of circumstellar gas around massive stars. I. The impact of the time sequence Ostar -> LBV -> WR star. A&A 305:229

Garcia-Segura G, Langer N, Mac Low MM (1996) The hydrodynamic evolution of circumstellar gas around massive stars. II. The impact of the time sequence O star -> RSG -> WR star. A&A 316:133–146

Gehrels N, Laird MC, Jackman HC, Cannizzo KJ, Mattson JB, Chen W (2003) Ozone depletion from nearby supernovae. ApJ 585:1169–1176

Grenier IA (2004) The Gould Belt, star formation, and the local interstellar medium. ArXiv Astrophys e-prints, arXiv:astro-ph/0409096

Gry C, Nehmé C, Boulanger F, Lebourlot J, Des Forêts GP, Falgarone E (2009) Supernova impact on a molecular cloud in the local bubble. In: Smith KR, Snowden LS, Kuntz KD (eds) American institute of physics conference series, vol 1156, pp 218–222. doi:10.1063/1.3211817

Gry C, Jenkins BE (2014) The interstellar cloud surrounding the Sun: a new perspective. A&A 567:A58. doi:10.1051/0004-6361/201323342

Gloeckler G, Fisk L (2007) Johannes Geiss' investigations of solar, heliospheric and interstellar matter. Space Sci Rev 27:489–513

Hanayama H, Tomisaka K (2006) Long-term evolution of supernova remnants in magnetized interstellar medium. ApJ 641:905–918. doi:10.1086/500527

Hanbury Brown R, Davies DR, Hazard C (1960) A curious feature of the radio sky. Obs 80: 191–198

Heerikhuisen J, Pogorelov NV, Zank GP, Crew GB, Frisch PC, Funsten HO, Janzen PH, McComas DJ, Reisenfeld DB, Schwadron NA (2010) Pick-up ions in the outer heliosheath: a possible mechanism for the interstellar boundary eXplorer ribbon. ApJ Lett 708:L126–L130

Herbig HG (1968) The interstellar line spectrum of zeta Oph. Zeitschrift Astrophysics 68: 243–277

Heiles C (1979) H I shells and supershells. ApJ 229:533–537

Heiles C, Chu Y, Troland HT, Reynolds JR, Yegingil I (1980) A new look at the North Polar Spur. ApJ 242:533–540

Heiles C (1984) H I shells, supershells, shell-like objects, and 'worms'. ApJS 55:585–595

Heiles C (1989) Magnetic fields, pressures, and thermally unstable gas in prominent H I shells. ApJ 336:808–821

Heiles C, Reach TW, Koo CB (1996) Radio recombination lines from inner galaxy diffuse gas. II. The extended low-density warm ionized medium and the "Worm-ionized Medium". ApJ 466:191

Heiles C (1998) Whence the Local Bubble, Gum, Orion? GSH 238+00+09, a nearby major superbubble toward galactic longitude 238 degrees. ApJ 498:689–703

Heiles C, Haffner ML, Reynolds JR (1999) The Eridanus superbubble in its multiwavelength glory. In: Taylor RA, Landecker LT, Joncas G (eds) New perspectives on the interstellar medium. Astronomical Society of the Pacific conference series, vol 168. Astronomical Society of the Pacific, San Francisco, p 211

Holzer TE (1989) Interaction between the solar wind and the interstellar medium. Ann Rev Astron Astrophys 27: 199–234

Hoyle F, Lyttleton RA (1939) The effect of interstellar matter on climatic variation. Proc Camb Philol Soc 35:405. doi:10.1017/S0305004100021150

Iwan DC (1980) X-ray observations of the North Polar Spur. ApJ 239:316–327

Jenkins BE (2009) A unified representation of gas-phase element depletions in the interstellar medium. ApJ 700:1299–1348

Jones AP, Tielens AGGM, Hollenbach DJ, McKee CF (1994) Grain destruction in shocks in the interstellar medium. ApJ 433:797–810

Jones AP, Tielens A, Hollenbach DJ (1996) Grain shattering in shocks: the interstellar grain size distribution. ApJ 469:740–764

Kimura H, Mann I, Jessberger KE (2003) Elemental abundances and mass densities of dust and gas in the local interstellar cloud. ApJ 582:846–856

Knie K, Korschinek G, Faestermann T, Wallner C, Scholten J, Hillebrandt W (1999) Indication for supernova produced ^{60}Fe activity on Earth. Phys Rev Lett 83:18–21. doi:10.1103/PhysRevLett.83.18

Knie K, Korschinek G, Faestermann T, Dorfi AE, Rugel G, Wallner A (2004) ^{60}Fe anomaly in a deep-sea manganese crust and implications for a nearby supernova source. Phys Rev Lett 93(17):171103. doi:10.1103/PhysRevLett.93.171103

Knödlseder J (1999) Gamma rays: observations, nuclear reactions, nucleosynthesis, abundances, stars: wolf-rayet, stars: supernovae: general. ApJ 510:915–929. doi:10.1086/306601

Knödlseder J, Bennett K, Bloemen H, Diehl R, Hermsen W, Oberlack U, Ryan J, Schönfelder V, von Ballmoos P (1999) A multiwavelength comparison of COMPTEL 1.8 MeV {(26) } line data. A&A 344:68–82

Koo CB, McKee FC (1992a) Dynamics of wind bubbles and superbubbles. I – slow winds and fast winds. II – analytic theory. ApJ 388:93–126. doi:10.1086/171132

Koo CB, McKee FC (1992b) Dynamics of Wind Bubbles and Superbubbles. II. Analytic Theory. ApJ 388:103. doi:10.1086/171133

Korpi JM, Brandenburg A, Shukurov A, Tuominen I (1999) Evolution of a superbubble in a turbulent, multi-phased and magnetized ISM. A&A 350:230–239

Koutroumpa D, Lallement R, Raymond CJ, Kharchenko V (2009) The solar wind charge-transfer X-ray emission in the 1/4 keV energy range: inferences on local bubble hot gas at low Z. ApJ 696:1517–1525. doi:10.1088/0004-637X/696/2/1517

Krause MGH, Diehl R, Bagetakos Y, Brinks E, Burkert A, Gerhard O, Greiner J, Kretschmer K, Siegert T (2015) ^{26}Al kinematics: superbubbles following the spiral arms? Constraints from the statistics of star clusters and HI supershells. A&A 578:A113. doi:10.1051/0004-6361/201525847

Kubiak AM, Swaczyna P, Bzowski M, Sokół JM, Fuselier SA, Galli A, Heirtzler D, Kucharek H, Leonard WT, McComas DJ, Möbius E, Park J, Schwadron AN, Wurz P (2016) Interstellar neutral helium in the heliosphere from IBEX observations. IV. Flow vector, Mach number, and abundance of the warm breeze. ApJS 223:25. doi:10.3847/0067-0049/223/2/25

Kun M (2007) The enigmatic loop III and the local galactic structure. In: Elmegreen GB, Palous J (eds) Triggered star formation in a turbulent ISM. IAU symposium, vol 237, pp 119–123. doi:10.1017/S1743921307001329

Kuntz DK, Collado-Vega YM, Collier RM, Connor KH, Cravens TE, Koutroumpa D, Porter SF, Robertson PI, Sibeck GD, Snowden LS, Thomas EN, Walsh MB (2015) The solar wind charge-exchange production factor for hydrogen. ApJ 808:143. doi:10.1088/0004-637X/808/2/143

Lallement R, Snowden S, Kuntz DK, Dame MT, Koutroumpa D, Grenier I, Casandjian MJ (2016) On the distance to the North Polar Spur and the local CO-H2 factor. Astron Astrophys 595:A131. ArXiv e-prints

Lallement R, Vidal-Madjar A, Ferlet R (1986) Multi-component velocity structure of the local interstellar medium. Astron Astrophys 168:225–236

Leske AR (2000) Anomalous cosmic ray composition from ACE. In: Dingus BL, Kieda BD, Salamon MH (eds) 26th International Cosmic Ray Conference, ICRC XXVI. American Institute of Physics Conference Series, vol 516, pp 274–282. doi:10.1063/1.1291481

Limongi M, Chieffi A (2003) Evolution, explosion, and nucleosynthesis of core-collapse supernovae. ApJ 592:404–433. doi:10.1086/375703

Ludwig P, Bishop S, Eglib R, Chernenkoa Vea (2016) Time-resolved 2-million-year-old supernova activity discovered in Earth's microfossil record. PNAS 113:9232–9237. doi:10.1073/pnas.1601040113

Maíz-Apelláriz J (2001) The origin of the local bubble. ApJ Lett 560:L83

Mac Low MM, McCray R (1988) Superbubbles in disk galaxies. ApJ 324:776–785. doi:10.1086/165936

Mac Low MM, McCray R, Norman LM (1989) Superbubble blowout dynamics. ApJ 337:141–154. doi:10.1086/167094

Mac Low MM (1999) The interaction of the disk with the Halo. In: Taylor RA, Landecker LT, Joncas G (eds) New perspectives on the interstellar medium. Astronomical Society of the Pacific conference series, vol 168. Astronomical Society of the Pacific, San Francisco, p 303

McCammon D, Burrows ND, Sanders TW, Kraushaar LW (1983) The Soft X-ray Diffuse Background. ApJ 269:107–135

McCammon D, Sanders TW (1990) The soft X-ray background and its origins. Ann Rev Astron Astrophys 28:657–688. doi:10.1146/annurev.aa.28.090190.003301

McComas DJ, Allegrini F, Bochsler P, Bzowski M, Christian ER, Crew GB, DeMajistre R, Fahr H, Fichtner H, Frisch PC, Funsten HO, Fuselier SA, Gloeckler G, Gruntman M, Heerikhuisen J, Izmodenov V, Janzen P, Knappenberger P, Krimigis S, Kucharek H, Lee M, Livadiotis G, Livi S, MacDowall RJ, Mitchell D, Möbius E, Moore T, Pogorelov NV,Reisenfeld D, Roelof E, Saul L, Schwadron NA, Valek PW,Vanderspek R, Wurz P, Zank GP (2009) Comparison of interstellar boundary explorer observations with 3D global heliospheric models. Science 326:959

McComas JD, Lewis SW, Schwadron AN (2014) IBEXs Enigmatic Ribbon in the sky and its many possible sources. Rev Geophys 52:118–155. doi:10.1002/2013RG000438

McComas JD, Bzowski M, Frisch P, Fuselier AS, Kubiak AM, Kucharek H, Leonard T, Möbius E, Schwadron AN, Sokół JM, Swaczyna P, Witte M (2015a) Warmer local interstellar medium: a possible resolution of the Ulysses-IBEX Enigma. ApJ 801:28. doi:10.1088/0004-637X/801/1/28

McComas JD, Bzowski M, Fuselier AS, Frisch CP, Galli A, Izmodenov VV, Katushkina AO, Kubiak AM, Lee AM, Leonard WT, Möbius E, Park J, Schwadron AN, Sokół JM, Swaczyna P, Wood EB, Wurz P (2015b) Local interstellar medium: six years of direct sampling by IBEX. ApJS 220:22. doi:10.1088/0067-0049/220/2/22

McKee FC, van Buren D, Lazareff B (1984) Photoionized stellar wind bubbles in a cloudy medium. ApJ Lett 278:L115–L118. doi:10.1086/184237

Meyer DM, Lauroesch JT, Peek JEG, Heiles C (2012) The remarkable high pressure of the local leo cold cloud. ApJ 752:119. doi:10.1088/0004-637X/752/2/119

Möbius E, Bochsler P, Bzowski M, Crew BG, Funsten OH, Fuselier SA, Ghielmetti A, Heirtzler D, Izmodenov VV, Kubiak M, Kucharek H, Lee AM, Leonard T, McComas JD, Petersen L, Saul L, Scheer AJ, Schwadron N, Witte M, Wurz P (2009) Direct observations of interstellar H, He, and O by the interstellar boundary explorer. Science 326:969-. doi:10.1126/science.1180971

Müller HR, Frisch PC, Florinski V, Zank GP (2006) Heliospheric response to different possible interstellar environments. ApJ 647:1491–1505

Müller HR, Frisch PC, Fields BD, Zank GP (2009) The heliosphere in time. Space Sci Rev 143:415–425

Murphy RP, Sasaki M, Binns WR, Brandt TJ, Hams T, Israel MH, Labrador AW, Link JT, Mewaldt RA, Mitchell JW, Rauch BF, Sakai K, Stone EC, Waddington CJ, Walsh NE, Ward JE, Wiedenbeck ME (2016) Galactic cosmic ray origins and OB associations: evidence from SuperTIGER observations of elements _26Fe through _40Zr. ArXiv e-prints

Nehmé C, Gry C, Boulanger F, Le Bourlot J, Pineau Des Forêts G, Falgarone E (2008) Multi-wavelength observations of a nearby multi-phase interstellar cloud. A&A 483:471–484. doi:10.1051/0004-6361:20078373

Neronov A, Meynet G (2016) Abundances of ^{59}Co and ^{59}Ni in the cosmic ray flux. A&A 588:A86. doi:10.1051/0004-6361/201527762

Ochsendorf BB, Brown AGA, Bally J, Tielens AGMG (2015) Nested shells reveal the rejuvenation of the Orion-Eridanus Superbubble. ApJ 808:111. doi:10.1088/0004-637X/808/2/111

Oey SM, García-Segura G (2004) Ambient interstellar pressure and superbubble evolution. ApJ 613:302–311. doi:10.1086/421483

Park J, Kucharek H, Möbius E (2014) The Ne-to-O abundance ratio of the interstellar medium from IBEX-Lo observations. ApJ 795:97

Park J, Kucharek H, Möbius E, Galli A, Livadiotis G, Fuselier SA, McComas JD (2015) Statistical analysis of the heavy neutral atoms measured by IBEX. ApJS 220:34. doi:10.1088/0067-0049/220/2/34

Peek JEG, Heiles C, Peek KMG, Meyer DM, Lauroesch JT (2011) The local leo cold cloud and new limits on a local hot bubble. ApJ 735:129. doi:10.1088/0004-637X/735/2/129

Pellizza JL, Mignani PR, Grenier AI, Mirabel IF (2005) On the local birth place of Geminga. A&A 435:625–630

Perrot CA, Grenier IA (2003) 3D dynamical evolution of the interstellar gas in the Gould Belt. A&A 404:519–531. doi:10.1051/0004-6361:20030477

Pogorelov NV, Suess ST, Borovikov SN, Ebert RW, McComas DJ, Zank GP (2013) Three-dimensional features of the outer heliosphere due to coupling between the interstellar and interplanetary magnetic fields. IV. solar cycle model based on Ulysses observations.ApJ 772:2. doi:10.1088/0004-637X/772/1/2

Pon A, Ochsendorf BB, Alves J, Bally J, Basu S, Tielens AGGM (2016) Kompaneets model fitting of the Orion-Eridanus Superbubble. II. thinking outside of barnards loop. ApJ 827:42. doi:10.3847/0004-637X/827/1/42

Rauch BF, Link JT, Lodders K, Israel MH, Barbier LM, Binns WR, Christian ER, Cummings JR, de Nolfo GA, Geier S, Mewaldt RA, Mitchell JW, Schindler SM, Scott LM, Stone EC, Streitmatter RE, Waddington CJ, Wiedenbeck ME (2009) Cosmic ray origin in OB associations and preferential acceleration of refractory elements: evidence from abundances of elements $_{26}$Fe through $_{34}$Se. ApJ 697:2083–2088. doi:10.1088/0004-637X/697/2/2083

Redfield S, Linsky JL (2004) Structure of local interstellar medium. III. Temperature and turbulence. ApJ 613:1004–1022

Redfield S, Linsky LJ (2008) The structure of the local interstellar medium. IV. Dynamics, morphology, physical properties, and implications of cloud-cloud interactions. ApJ 673: 283–314

Reynolds JR (1984) Optical emission line studies and the warm, ionized component of the local interstellar medium. In: Kondo Y, Bruhweiler CF, Savage BD (eds) NASA conference publication, vol 2345. NASA, Goddard

Rogerson JB, York DG, Drake JF, Jenkins EB, Morton DC, Spitzer L (1973) Spectrophotometric results from the copernicus satellite. III. Ionization and composition of the intercloud medium. ApJ Lett 181:L110. doi:10.1086/181196

Routly P, Spitzer JL (1952) A comparison of the components in interstellar sodium and calcium. ApJ 115:227

Rozyczka M, Tenorio-Tagle G, Franco J, Bodenheimer P (1993) On the evolution of supernova remnants. III - Off-centred supernova explosions in pre-existing wind-driven bubbles. MNRAS 261:674–680. doi:10.1093/mnras/261.3.674

Rugel G, Faestermann T, Knie K, Korschinek G, Poutivtsev M, Schumann D, Kivel N, Günther-Leopold I, Weinreich R, Wohlmuther M (2009) New measurement of the Fe60 half-life. Phys Rev Lett 103(7):072502. doi:10.1103/PhysRevLett.103.072502

Salter JC (1983) Loop-I the North Polar Spur – a major feature of the local interstellar environment. Bull Astron Soc India 11:1

Salvati M (2010) The local Galactic magnetic field in the direction of Geminga. A&A 513:A28+

Sanders TW, Kraushaar LW, Nousek AJ, Fried MP (1977) Soft diffuse X-rays in the southern galactic hemisphere. ApJ Lett 217:L87–L91. doi:10.1086/182545

Santos PF, Corradi W, Reis W (2011) Optical polarization mapping toward the interface between the local cavity and Loop I. ApJ 728:104

Scherer K, Fichtner H, Borrmann T, Beer J, Desorgher L, Flükiger E, Fahr HJ, Ferreira SES, Langner UW, Potgieter MS, Heber B, Masarik J, Shaviv N, Veizer J (2006) Interstellar-terrestrial relations: variable cosmic environments, the dynamic heliosphere,

and their imprints on terrestrial archives and climate. Space Sci Rev 127:327–465. doi:10.1007/s11214-006-9126-6

Schwadron AN, Adams CF, Christian RE, Desiati P, Frisch P, Funsten OH, Jokipii RJ, McComas JD, Moebius E, Zank PG (2014) Global anisotropies in TeV cosmic rays related to the Suns local galactic environment from IBEX. Science 343:988–990. doi:10.1126/science.1245026

Schwadron NA, Allegrini F, Bzowski M, Christian ER, Crew GB, Dayeh M, DeMajistre R, Frisch P, Funsten HO, Fuselier SA, Goodrich K, Gruntman M, Janzen P, Kucharek H, Livadiotis G, McComas DJ, Moebius E, Prested C, Reisenfeld D, Reno M, Roelof E, Siegel J, Vanderspek R (2011) Separation of the interstellar boundary explorer ribbon from globally distributed energetic neutral atom flux. ApJ 731:56–77. doi:10.1088/0004-637X/731/1/56

Schwadron NA, Bzowski M, Crew GB, Gruntman M, Fahr H, Fichtner H, Frisch PC, Funsten HO, Fuselier S, Heerikhuisen J, Izmodenov V, Kucharek H, Lee M, Livadiotis G, McComas DJ, Moebius E, Moore T, Mukherjee J, Pogorelov NV, Prested C, Reisenfeld D, Roelof E, Zank GP (2009) Comparison of interstellar boundary explorer observations with 3D global heliospheric models. Science 326:966-

Schwadron AN, McComas JD (2013) Spatial retention of ions producing the IBEX ribbon. ApJ 764:92. doi:10.1088/0004-637X/764/1/92

Schwadron AN, Moebius E, Kucharek H, Lee AM, French J, Saul L, Wurz P, Bzowski M, Fuselier AS, Livadiotis G, McComas DJ, Frisch P, Gruntman M, Mueller RH (2013) Determination of interstellar He parameters using five years of data from the interstellar boundary explorer: beyond closed form approximations. ApJ 775:86. doi:10.1088/0004-637X/775/2/86

Schwadron AN, Moebius E, Leonard T, Fuselier AS, McComas JD, Heirtzler D, Kucharek H, Rahmanifard F, Bzowski M, Kubiak AM, Sokol J, Swaczyna P, Frisch P (2015) Determination of interstellar He parameters using five years of data from the interstellar boundary explorer: beyond closed form approximations. ApJS 220:25. doi:10.1088/0067-0049/220/2/25

Schwadron AN, Möbius E, McComas JD, Bochsler P, Bzowski M, Fuselier AS, Livadiotis G, Frisch P, Müller HR, Heirtzler D, Kucharek H, Lee A (2016) Determination of interstellar oxygen parameters using the first two years of data from the interstellar boundary explorer. ApJ 828:81. doi:10.3847/0004-637X/828/2/81

Sembach RK, Danks CA (1994) Optical studies of interstellar material in low density regions of the Galaxy. A&A 289:539–558

Shapley H (1921) Note on a possible factor in changes of geological climate. J Geology 29: 502–504

Shull MJ (1993) Hot phases or the interstellar medium, stellar winds, supernovae, and turbulent mixing layers. In: Cassinelli PJ, Churchwell EB (eds) Massive stars: their lives in the interstellar medium. Astronomical Society of the Pacific conference series, vol 35. Astronomical Society of the Pacific, San Francisco, p 327

Siluk SR, Silk J (1974) On the velocity dependence of the interstellar Na I/Ca II ratio. ApJ 192:51–57

Slavin JD (1989) Consequences of a conductive boundary on the local cloud. I – No Dust. ApJ 346:718-727

Slavin JD, Dwek E, Jones PA (2015) Destruction of interstellar dust in evolving supernova remnant shock waves. ApJ 803:7. doi:10.1088/0004-637X/803/1/7

Slavin JD, Frisch PC (1996) Relative ionizations in the nearest interstellar gas. Space Sci Rev 78:223–228

Slavin JD, Frisch C (2002) The ionization of nearby interstellar gas. ApJ 565:364–379

Slavin JD, Frisch PC (2008) The boundary conditions of the heliosphere: photoionization models constrained by interstellar and in situ data. A&A 491:53–68

Smith KR, Cox PD (2001) Multiple supernova remnant models of the local bubble and the soft X-ray background. ApJS 134:283–309. doi:10.1086/320850

Smith VV, Cunha K, Plez B (1994) Is Geminga a runaway member of the Orion association?. A&A 281:L41–L44

Smith KR, Foster RA, Edgar JR, Brickhouse SN (2014) Resolving the origin of the diffuse soft X-ray background. ApJ 787:77. doi:10.1088/0004-637X/787/1/77

Snowden LS, Heiles C, Koutroumpa D, Kuntz DK, Lallement R, McCammon D, Peek JGE (2015) Revisiting the local leo cold cloud and revised constraints on the local hot bubble. ApJ 806:119. doi:10.1088/0004-637X/806/1/119

Snowden LS, Koutroumpa D, Kuntz DK, Lallement R, Puspitarini L (2015) The north galactic pole rift and the local hot bubble. ApJ 806:120. doi:10.1088/0004-637X/806/1/120

Sofue Y (2015) The North Polar Spur and Aquila Rift. MNRAS 447:3824–3831. doi:10.1093/mnras/stu2661

Spitzer L (1976) High-velocity interstellar clouds. Comments Astrophys 6:177–187

Spoelstra TAT (1972) A survey of linear polarization at 1415 MHz. IV. Discussion of the results for the galactic spurs. A&A 21:61

Sterken JV, Strub P, Krüger H, von Steiger R, Frisch P (2015) Sixteen years of Ulysses interstellar dust measurements in the solar system. III. Simulations and data unveil new insights into local interstellar dust. ApJ 812:141

Stothers R, Frogel JA (1974) The local complex of 0 and B stars. I. Distribution of stars and interstellar dust. AJ 79:456

Su M, Slatyer RT, Finkbeiner PD (2010) Giant gamma-ray bubbles from Fermi-Lat. ApJ 724:1044–1082

Sun HX, Landecker LT, Gaensler MB, Carretti E, Reich W, Leahy JP, McClure-Griffiths NM, Crocker MR, Wolleben M, Haverkorn M, Douglas AK, Gray DA (2015) Faraday tomography of the North Polar Spur: constraints on the distance to the Spur and on the magnetic field of the galaxy. ApJ 811:40. doi:10.1088/0004-637X/811/1/40

Tenorio-Tagle G, Rozyczka M, Franco J, Bodenheimer P (1991) On the evolution of supernova remnants. II - Two-dimensional calculations of explosions inside pre-existing wind-driven bubbles. MNRAS 251:318–329. doi:10.1093/mnras/251.2.318

Tenorio-Tagle G, Bodenheimer P, Franco J, Rozyczka M (1990) On the evolution of super-nova remnants. I - Explosions inside pre-existing wind-driven bubbles. MNRAS 244: 563–576.

Tetzlaff N, Torres G, Neuhäuser R, Hohle MM (2013) The neutron star born in the Antlia supernova remnant. MNRAS 435:879–884. doi:10.1093/mnras/stt1358

Toalá JA, Guerrero AM, Chu HY, Gruendl AR (2015) On the diffuse X-ray emission from the Wolf-Rayet bubble NGC 2359. MNRAS 446:1083–1089. doi:10.1093/mnras/stu2163

Toalá JA, Guerrero AM, Chu HY, Arthur JS, Tafoya D, Gruendl RA (2016) X-ray emission from the Wolf-Rayet bubble NGC 6888 – II. XMM-Newton EPIC observations. MNRAS 456: 4305–4314. doi:10.1093/mnras/stv2819

Toalá JA, Arthur JS (2011) Radiation-hydrodynamic Models of the evolving circumstellar medium around massive Stars. ApJ 737:100. doi:10.1088/0004-637X/737/2/100

van Marle AJ, Smith N, Owocki PS, van Veelen B (2010) Numerical models of collisions between core-collapse supernovae and circumstellar shells. MNRAS 407:2305–2327. doi:10.1111/j.1365-2966.2010.16851.x

van Marle AJ, Meliani Z, Marcowith A (2015) Shape and evolution of wind-blown bubbles of massive stars: on the effect of the interstellar magnetic field. A&A 584:A49. doi:10.1051/0004-6361/201425230

Vidal M, Dickinson C, Davies DR, Leahy PJ (2015) Polarized radio filaments outside the galactic plane. MNRAS 452:656–675. doi:10.1093/mnras/stv1328

Wallner A, Feige J, Kinoshita N, Paul M, Fifield KL, Golser R, Honda M, Linnemann U, Matsuzaki H, Merchel S, Rugel G, Tims GS, Steier P, Yamagata T, Winkler RS (2016) Recent near-Earth supernovae probed by global deposition of interstellar radioactive ^{60}Fe. Nature 532:69–72. doi:10.1038/nature17196

Washimi H, Tanaka T (1999) MHD structure of the heliosphere and its response to the 11-year solar cycle variations. Adv Space Res 23:551–560

Weaver R, McCray R, Castor J, Shapiro P, Moore R (1977) Interstellar bubbles. II - Structure and evolution. ApJ 218:377–395. doi:10.1086/155692

Welsh YB, Shelton LR (2009) The trouble with the local bubble. Ap&SS 323:1–16. doi:10.1007/s10509-009-0053-3

Welty ED, Hobbs ML, Lauroesch TJ, Morton CD, Spitzer L, York DG (1999) The diffuse interstellar clouds toward 23 Orionis. ApJS 124:465–501

Welty ED, Jenkins BE, Raymond CJ, Mallouris C, York GD (2002) ApJ 579:304

Wiedenbeck ME, Binns WR, Christian ER, Cummings AC, Dougherty BL, Hink PL, Klarmann J, Leske RA, Lijowski M, Mewaldt RA, Stone EC, Thayer MR, von Rosenvinge TT, Yanasak NE (1999) Constraints on the time delay between nucleosynthesis and cosmic-ray acceleration from observations of ^{59}Ni and ^{59}Co. ApJ Lett 523:L61–L64. doi:10.1086/312242

Williamson OF, Sanders TW, Kraushaar LW, McCammon D, Borken R, Bunner NA (1974) Observation of features in the soft X-ray background flux. ApJ Lett 193:L133–L137. doi:10.1086/181649

Witte M (2004) Kinetic parameters of interstellar neutral helium. Review of results obtained during one solar cycle with the Ulysses/GAS-instrument. A&A 426:835–844. doi:10.1051/0004-6361:20035956

Wolff B, Koester D (1999) Lallement R Evidence for an ionization gradient in the local interstellar medium: EUVE observations of white dwarfs. A&A 346:969

Wolleben M (2007) A new model for the Loop I (North Polar Spur) region. ApJ 664:349–356. doi:10.1086/518711

Yadav N, Mukherjee D, Sharma P, Nath BB (2016) Supernovae under microscope: how supernovae overlap to form superbubbles. ArXiv e-prints

Zank GP (2015) Faltering steps into the galaxy: the boundary regions of the heliosphere. Ann Rev Astron Astrophys 53:449-500. doi:10.1146/annurev-astro-082214-122254

Zank GP, Frisch PC ApJ (1999) Consequences of a change in the galactic environment of the sun. 518:965–973

Zirnstein EJ, Heerikhuisen J, Funsten HO, Livadiotis G, McComas DJ, Pogorelov NV (2016) Local interstellar magnetic field determined from the interstellar boundary explorer ribbon. ApJ Lett 818:L18. doi:10.3847/2041-8205/818/1/L18